

A Jacobi Diagonalization and Anderson Acceleration Algorithm For Variational Quantum Algorithm Parameter Optimization

Robert M. Parrish,^{1,*} Joseph T. Iosue,¹ Asier Ozaeta,¹ and Peter L. McMahon^{2,1}

¹ *QC Ware Corporation, Palo Alto, CA 94301*

² *E. L. Ginzton Laboratory, Stanford University, Stanford, CA 94305*

The optimization of circuit parameters of variational quantum algorithms such as the variational quantum eigensolver (VQE) or the quantum approximate optimization algorithm (QAOA) is a key challenge for the practical deployment of near-term quantum computing algorithms. Here, we develop a hybrid quantum/classical optimization procedure inspired by the Jacobi diagonalization algorithm for classical eigendecomposition, and combined with Anderson acceleration. In the first stage, analytical tomography fittings are performed for a local cluster of circuit parameters via sampling of the observable objective function at quadrature points in the circuit angles. Classical optimization is used to determine the optimal circuit parameters within the cluster, with the other circuit parameters frozen. Different clusters of circuit parameters are then optimized in “sweeps,” leading to a monotonically-convergent fixed-point procedure. In the second stage, the iterative history of the fixed-point Jacobi procedure is used to accelerate the convergence by applying Anderson acceleration/Pulay’s direct inversion of the iterative subspace (DIIS). This Jacobi+Anderson method is numerically tested using a quantum circuit simulator (without noise) for a representative test case from the multistate, contracted variant of the variational quantum eigensolver (MC-VQE), and is found to be competitive with and often faster than Powell’s method and L-BFGS.

I. INTRODUCTION

The past few years have witnessed the arrival of a wave of hybrid quantum/classical algorithms^{1,2} with compelling properties for use on noisy intermediate-scale quantum (NISQ) devices.³ A universal feature of these methods is that they involve the hybrid quantum/classical optimization of a real quantum observable expectation value \mathcal{O} with respect to a polynomial number of quantum circuit parameters $\{\theta_g\}$. For a given set of circuit parameters, the quantum observable expectation value can be determined by statistically sampling the output measurements of the quantum circuit,

$$\mathcal{O}(\{\theta_g\}) = \langle \vec{0} | \hat{U}^\dagger(\{\theta_g\}) \hat{O} \hat{U}(\{\theta_g\}) | \vec{0} \rangle \quad (1)$$

$$= \sum_k \gamma_k(\{\theta_g\}) h_k \quad (2)$$

Here $|\vec{0}\rangle$ is the all-zeros starting qubit state for N qubits, $\hat{U}(\{\theta_g\})$ is the 2^N -dimensional Hilbert space unitary operator parameterized by the quantum circuit, and \hat{O} is a Hermitian operator defining the desired quantum observable expectation value. Generally \hat{O} is defined in a problem-specific way in terms of a polynomial number of Pauli strings $\{\hat{P}_k\}$ accompanied by problem-specific matrix elements $\{h_k\}$ (determined classically before the quantum algorithm is applied),

$$\hat{O} \equiv \sum_k h_k \hat{P}_k \quad (3)$$

In practice, statistical observation of the quantum circuit is used to determine the density matrix elements,

$$\gamma_k \equiv \langle \vec{0} | \hat{U}^\dagger(\{\theta_g\}) \hat{P}_k \hat{U}(\{\theta_g\}) | \vec{0} \rangle \quad (4)$$

These are subsequently contracted classically with the matrix elements $\{h_k\}$ as in Equation 2. At this point, we have a recipe (which involves repeatedly observing the output of a quantum circuit) for the evaluation of the observable expectation value \mathcal{O} at a given set of circuit parameters $\{\theta_g\}$. The remaining task, and the major driver for this study, is to classically optimize the N_g -dimensional objective function $\mathcal{O}(\{\theta_g\})$ with as few observable expectation value evaluations as possible, and in the presence of both statistical and physical-device-imperfection noise channels.

Quantum methods of this class include the variational quantum eigensolver^{1,4–8} (VQE) and the quantum approximate optimization algorithm² (QAOA). VQE was initially developed for quantum chemistry applications such as the approximation of the ground-state energy of the electronic wavefunction of small molecular complexes. VQE has since seen widespread extension of application to the simulation of electronic, magnetic, and excitonic Hamiltonians. Extensions to VQE such as the folded spectrum,¹ orthogonality-constrained^{9,10} (OC-VQE), quantum subspace expansion^{11,12} (QSE-VQE), the subspace search¹³ (SS-VQE), and multi-state, contracted¹⁴ (MC-VQE) extensions have enabled the computation of excited states^{9–14} and transition properties.¹⁴ A recent advance has even enabled a post-quantum classical correction from perturbation theory to enhance the accuracy of the method.¹⁵ VQE and its extensions have been deployed on physical quantum hardware to simulate the ground and excited-state energies of small molecules and magnetic systems, including deployment on superconducting^{1,6,12} and ion-trap¹⁶ quantum hardware.

The quantum approximate optimization algorithm² (QAOA) is another prominent variational quantum algorithm; it is designed to try solve classical combinatorial-

optimization problems over binary variables, such as MAX-CUT or classical Ising optimization. QAOA uses alternating unitary evolutions of a cost-function Hamiltonian and a driver Hamiltonian, and canonically each evolution unitary has associated with it a real-valued parameter. It is these parameters that are varied in an attempt to have the circuit return optimal choices for the binary variables. QAOA has broad potential application due partially to the fact that many NP-hard optimization problems can be mapped to Ising form with low overhead,^{17,18} or variations of QAOA may more directly allow solution of constrained binary optimization problems.¹⁹ Much of the recent body of work exploring use cases for quantum annealing is also directly relevant to QAOA, since it focuses on problems that can be mapped to Ising form.^{20–22} While some initial implementations of QAOA used off-the-shelf gradient-free classical optimization methods,^{23,24} a substantial body of work has developed exploring off-the-shelf and customized use of gradient-free and gradient-based methods.^{25–29} There has also been recent work that systematically compares six off-the-shelf optimization methods for QAOA.³⁰

Methods for optimizing variational circuits using analytical gradients have also seen rapid development over the past two years^{31–36}. These techniques have been applied to examples in QAOA, VQE, as well as machine learning (in particular, quantum neural networks). It has also recently been noted that variational methods on random quantum circuits may suffer from “barren plateaus” filled with vanishing gradients;³⁷ this needs to be taken into consideration when using gradient-based methods.

The inspiration for the methods we develop in this work is a much older class of optimization/root-finding algorithms: classical fixed point methods. One key method within this class is the Jacobi algorithm for the classical diagonalization of symmetric matrices,³⁸ depicted in Figure 1. The Jacobi diagonalization fixed-point iteration works by successively identifying an (i, j) “pivot index” within matrix \hat{A} , and then applying an orthogonal transformation by a Givens matrix to zero the off-diagonal element A_{ij} – i.e., exactly solving a local 2×2 subproblem. This is equivalent to diagonalizing the 2×2 submatrix of \hat{A} corresponding to A_{ii} , A_{ij} and A_{jj} , for which the angle of the Givens matrix can be determined analytically. In the process, the other elements of the i -th and j -th rows and columns of \hat{A} are mixed. This local optimization can then be repeated across different sequences of (i, j) pivot indices, hopefully making progress toward global diagonalization of \hat{A} . Of note, each discrete (i, j) optimization move is negative definite, so the overall algorithm converges monotonically. Many possible choices for the selection of the sequence of (i, j) pivots exist: Searching the matrix at each step for the largest off-diagonal element $|A_{ij}|$ to determine the (i, j) pivot yields the fastest convergence rates, but the search itself can be prohibitively expensive. Randomized (i, j) selection is often used, though it introduces nondeterminism into the fixed-point proce-

cedure (which will make forthcoming convergence acceleration procedures difficult to apply). Alternatively, simply “sweeping” over all of the $(i > j)$ pairs in a predetermined order often provides acceptable convergence within a simple and deterministic recipe. In practice, the Jacobi diagonalization algorithm converges rapidly for diagonally dominant matrices, and has compelling features for classical parallelization, though QR-based methods have generally superseded Jacobi methods for dense diagonalization on classical computing hardware.³⁹ The Jacobi diagonalization algorithm has been extended to Hermitian and non-Hermitian matrices and to singular value decomposition.⁴⁰ The Jacobi diagonalization algorithm is also widely used in the approximate simultaneous diagonalization of multiple matrices,^{41,42} e.g., in domain applications in orbital localization,^{43–46} and discrete variable representation grid determination,^{47–50} in computational chemistry.

The obvious disadvantage of local-move fixed-point algorithms like the Jacobi diagonalization algorithm is that while each local move is optimal for the given subproblem, the aggregate set of local moves are not necessarily cooperative with respect to the global problem. This can lead to slow though definitionally monotonic convergence. For instance, two or more different pivots may “slosh” off-diagonal weight back and forth in a way that does not promote rapid global convergence. To combat this, one can imagine extending the Jacobi diagonalization algorithm to pairs, clusters, or even large subblocks of the overall matrix. In practice, this often promotes more-rapid global convergence at the cost of much more involved computations for the solution of each local pair, cluster, or subblock solution. Moreover, the selection of the sets of pivot clusters generally requires heuristics or special knowledge of the structure of the problem. We will pursue a cluster approach below, but note that one more piece is needed to complete the recipe: some procedure which develops an effective or approximate global picture of the couplings between all pivot or cluster moves within a Jacobi sweep, and which promotes global cooperation between these moves.

Such a procedure is the fixed-point algorithm *doppelgänger* of Krylov subspace methods for iterative linear algebra problems or low-rank Hessian updating approaches in quasi-Newton approximation methods, but here the application is to sequence acceleration of a fixed-point-iteration method such as complete Jacobi sweeps. Numerous examples of such fixed-point acceleration methods exist in the mathematical physics literature, for example, Richardson extrapolation, Aitken’s delta-squared process, successive overrelaxation, and damping. One particularly compelling method is the class of fixed-point sequence acceleration methods developed by Anderson in 1965.⁵¹ Anderson acceleration has been applied in many domain problems in numerical science and engineering.⁵² Within the chemical physics literature, a highly similar acceleration method was independently developed by Pulay in 1980,⁵³ and extended

in 1982,⁵⁴ and is known as direct inversion of the iterative subspace (DIIS). DIIS is widely used to stabilize and accelerate the myriad classes of nonlinear equations appearing in electronic structure theory, notably the self-consistent field (SCF) equations,^{53–56} coupled cluster (CC) equations,⁵⁷ coupled-perturbed response equations, and even as an alternative to quasi-Newton methods for the optimization of molecular geometries.⁵⁸ All Anderson/Pulay DIIS sequence acceleration methods work by examining the iterative history of a sequence of state vectors (e.g., the circuit angles $\{\theta_g\}^k$ at each iteration k) and a corresponding sequence of approximate error vectors $\{\epsilon_g\}^k$. An improved/extrapolated state vector of the form $\{\theta_g\}'^k \equiv \sum_i c_i \{\theta_g\}^i$ is proposed, with the coefficients c_i chosen to minimize the sum of squares of the improved approximate error vector $\{\epsilon_g\}'^k \equiv \sum_i c_i \{\epsilon_g\}^i$, subject to the normalization constraint $\sum_i c_i = 1$. Many variations of Anderson and Pulay DIIS methods have been developed^{59–61} with different choices of approximate error vectors and placements within fixed-point iterative procedures.

In the present work, we develop a new local fixed-point-iteration plus global sequence acceleration optimization algorithm for general variational quantum circuit algorithms. First, we develop analytical formulae for the tomography of the observable expectation values as a function of a cluster of M circuit parameters. Together with a 3^M -point Fourier quadrature for the determination of the tomography parameters, this allows us to obtain partial tomography for each cluster of circuit parameters with a handful of observable evaluations at widely spaced angles. Next, we classically optimize the objective function within the tomography function for each cluster of angles. Then we sweep over different clusters of angles in a Jacobi-diagonalization-like fixed point procedure. Several sweep recipes are explored, such as all single-angle sweeps (Jacobi-1), all double-angle sweeps (Jacobi-2), and locally selected clusters based on quantum circuit structure (Jacobi-Gen), plus randomized-order extensions (e.g., Jacobi-1-Rand). We also augment the procedure with Anderson-type global sequence acceleration, using either the traditional Anderson-type recipe with the fixed-point move length as the error vector (Jacobi- F -Anderson) or the SCF Pulay DIIS-type recipe with the objective function gradient as the error vector (Jacobi- F -Pulay). We test the developed methods against Powell’s gradient-free conjugate direction method⁶² and the L-BFGS gradient-based quasi-Newton method⁶³ for MC-VQE+AIEM¹⁴ circuit parameter optimization for an $N = 4$ subset of bacteriochlorophylls in the B850 ring of LHII.

II. METHOD DEVELOPMENT

An overview of the family of Jacobi fixed point iteration plus Anderson/Pulay DIIS sequence acceleration

convergence algorithms developed herein is depicted in Figure 2. In the top panel, we develop methodology to perform tomography fitting of variational quantum circuits with respect to a subset of variational parameters. This involves the development of a simple analytical trigonometric form with problem-specific linear tomography parameters for the partial tomography of the observable expectation value with respect to the active cluster of parameters. The tomography parameters can be resolved by sampling the observable expectation value at widely spaced Fourier quadrature grid points, which are robust against cancellation error. Following the tomography fitting, classical optimization can be used to determine the optimal values of the active cluster of circuit parameters to arbitrary precision. In the middle panel, iterative sequences of these local moves are performed over different clusters of active parameters, yielding a monotonically-converging method that coarsely resembles classical Jacobi diagonalization. In the bottom panel, Anderson or Pulay DIIS sequence acceleration techniques are invoked to examine the iterative history of the Jacobi sweeps and propose modified sets of circuit parameters that promote cooperative optimization between the global set of circuit parameters.

In Section II.A, we gradually build up the tomography formulae and Fourier quadrature fitting procedures for various clusters and classes of quantum circuits. Specifically, Section II.A.1 covers the simplest $M = 1$ one-gate tomography (which required 3 quadrature points to resolve), Section II.A.2 covers the $M = 2$ double-gate tomography (which requires 9 quadrature points to resolve), Section II.A.3 covers the general M -gate tomography (which requires 3^M quadrature points to resolve), and Section II.A.4 covers the case encountered in QAOA where there are M clusters each of G gates with the same angle (which requires $(2G+1)^M$ quadrature points to resolve). In Section II.B, we describe a number of possible recipes for selecting the sequence of gate angle clusters to define each Jacobi sweep. In Section II.C, we describe two variants of Anderson acceleration approaches to improve global convergence properties of the approach: In Section II.C.1 we detail a traditional Anderson recipe where the error vector is taken to be the difference in the state vector between each move and the previous one, while in Section II.C.2 we detail a method that more closely resembles the Pulay DIIS procedure as commonly used in SCF theory, where the gradient is used as the error vector. In Section II.D, we comment on the similarity of Jacobi-1 and the Powell method.

In this work, we use the one-qubit $\hat{R}_y(\theta) \equiv e^{-i\theta\hat{Y}}$ gate as a universal gate for parameter entry.

A. VQE Tomography

1. One-Gate Tomography

Consider a general $1\text{-}\hat{R}_y$ -gate quantum circuit of the form encountered in VQE,



The corresponding observable expectation value is,

$$\mathcal{O}(\theta_A) \equiv \langle 0 | \hat{U}^\dagger \hat{R}_y^\dagger(\theta_A) \hat{V}^\dagger \hat{O} \hat{V} \hat{R}_y(\theta_A) \hat{U} | 0 \rangle \quad (6)$$

Here \hat{O} is a Hermitian operator, and \hat{U} and \hat{V} are unitary operators, all in the 2^N -dimensional Hilbert space for N qubits. These matrices are problem-specific, and their construction is determined classically before the invocation of the quantum algorithm. $\hat{R}_y(\theta_A) \equiv e^{-i\theta_A \hat{Y}_A}$ is a one-qubit rotation gate acting on an arbitrary qubit corresponding to index A . The observable expectation value $\mathcal{O}(\theta_A)$ is periodic for $\theta_A \in [-\pi/2, +\pi/2]$. By inspection, this has the definitional tomography,

$$\mathcal{O}(\theta_A) \equiv \alpha + \beta \cos(2\theta_A) + \gamma \sin(2\theta_A) \quad (7)$$

Here, $\{\alpha, \beta, \gamma\}$ are the “tomography parameters,” whose values depend on the specifics of the problem (i.e., the operators \hat{U} , \hat{V} , and \hat{O}). To determine the tomography parameters, we can define the three-point Fourier quadrature,

$$\mathcal{O}^- \equiv \mathcal{O}(-\pi/3), \quad \mathcal{O}^0 \equiv \mathcal{O}(0), \quad \mathcal{O}^+ \equiv \mathcal{O}(+\pi/3) \quad (8)$$

This has the matrix form,

$$\underbrace{\begin{bmatrix} 1 & -1/2 & -\sqrt{3}/2 \\ 1 & 1 & 0 \\ 1 & -1/2 & \sqrt{3}/2 \end{bmatrix}}_{\hat{T}_{(1)}} \begin{bmatrix} \alpha \\ \beta \\ \gamma \end{bmatrix} = \begin{bmatrix} \mathcal{O}^- \\ \mathcal{O}^0 \\ \mathcal{O}^+ \end{bmatrix} \quad (9)$$

The inverse is,

$$\hat{T}_{(1)}^{-1} = \frac{1}{3} \begin{bmatrix} 1 & 1 & 1 \\ -1 & 2 & -1 \\ -\sqrt{3} & 0 & \sqrt{3} \end{bmatrix} \quad (10)$$

The gradient is,

$$\mathcal{G}_A(\theta_A) \equiv \frac{\partial \mathcal{O}(\theta_A)}{\partial \theta_A} = -2\beta \sin(2\theta_A) + 2\gamma \cos(2\theta_A) \quad (11)$$

The Hessian is,

$$\mathcal{H}_{AA}(\theta_A) \equiv \frac{\partial^2 \mathcal{O}(\theta_A)}{\partial \theta_A^2} = -4\beta \cos(2\theta_A) - 4\gamma \sin(2\theta_A) \quad (12)$$

The stationary condition is,

$$\mathcal{G}_A(\theta_A) = 0 \Rightarrow \tan(2\theta_A) = \gamma/\beta \quad (13)$$

The minimal condition is,

$$\mathcal{H}_{AA}(\theta_A) \geq 0 \quad (14)$$

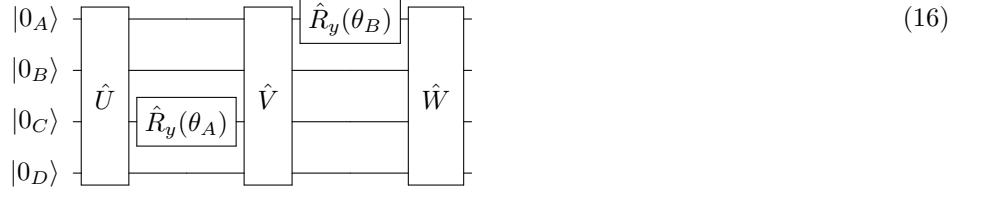
And the analytical solution for the optimal angle is therefore,

$$\Rightarrow \theta_A = \frac{1}{2} \arctan 2 \left(\frac{-\gamma}{-\beta} \right) \quad (15)$$

This solution is unique - there is only one local minimum in 1D.

2. Two-Gate Tomography

Now consider a general $2\text{-}\hat{R}_y$ -gate quantum circuit of the form encountered in VQE,



The corresponding observable expectation value is,

$$\mathcal{O}(\theta_A, \theta_B) \equiv \langle 0 | \hat{U}^\dagger \hat{R}_y^\dagger(\theta_A) \hat{V}^\dagger \hat{R}_y^\dagger(\theta_B) \hat{W}^\dagger \times \hat{O} \hat{W} \hat{R}_y(\theta_B) \hat{V} \hat{R}_y(\theta_A) \hat{U} | 0 \rangle \quad (17)$$

By inspection, this has the tomography,

$$\begin{aligned} \mathcal{O}(\theta_A, \theta_B) &\equiv \alpha\alpha + \alpha\beta \cos(2\theta_B) + \alpha\gamma \sin(2\theta_B) \\ &+ \beta\alpha \cos(2\theta_A) + \beta\beta \cos(2\theta_A) \cos(2\theta_B) + \beta\gamma \cos(2\theta_A) \sin(2\theta_B) \\ &+ \gamma\alpha \sin(2\theta_A) + \gamma\beta \sin(2\theta_A) \cos(2\theta_B) + \gamma\gamma \sin(2\theta_A) \sin(2\theta_B) \end{aligned} \quad (18)$$

We can define a nine-point Fourier quadrature,

$$\begin{aligned} \mathcal{O}^{--} &\equiv \mathcal{O}(-\pi/3, -\pi/3), \quad \mathcal{O}^{-0} \equiv \mathcal{O}(-\pi/3, 0), \\ \mathcal{O}^{-+} &\equiv \mathcal{O}(-\pi/3, +\pi/3), \quad \mathcal{O}^{0-} \equiv \mathcal{O}(0, -\pi/3), \\ \mathcal{O}^{00} &\equiv \mathcal{O}(0, 0), \quad \mathcal{O}^{0+} \equiv \mathcal{O}(0, +\pi/3), \\ \mathcal{O}^{+-} &\equiv \mathcal{O}(+\pi/3, -\pi/3), \quad \mathcal{O}^{+0} \equiv \mathcal{O}(+\pi/3, 0), \\ \mathcal{O}^{++} &\equiv \mathcal{O}(+\pi/3, +\pi/3), \end{aligned} \quad (19)$$

This has the matrix form,

$$\hat{T}_{(2)} \begin{bmatrix} \alpha\alpha \\ \alpha\beta \\ \alpha\gamma \\ \beta\alpha \\ \beta\beta \\ \beta\gamma \\ \gamma\alpha \\ \gamma\beta \\ \gamma\gamma \end{bmatrix} = \begin{bmatrix} \mathcal{O}^{--} \\ \mathcal{O}^{-0} \\ \mathcal{O}^{-+} \\ \mathcal{O}^{0-} \\ \mathcal{O}^{00} \\ \mathcal{O}^{0+} \\ \mathcal{O}^{+-} \\ \mathcal{O}^{+0} \\ \mathcal{O}^{++} \end{bmatrix} \quad (20)$$

Here $\hat{T}_{(2)} \equiv \hat{T}_{(1)} \otimes \hat{T}_{(1)}$ and the corresponding inverse is, $\hat{T}_{(2)}^{-1} = \hat{T}_{(1)}^{-1} \otimes \hat{T}_{(1)}^{-1}$.

The gradient is,

$$\mathcal{G}_A(\theta_A, \theta_B) \equiv \frac{\partial \mathcal{O}(\theta_A, \theta_B)}{\partial \theta_A}$$

$$= -2 \sin(2\theta_A) [\beta\alpha + \beta\beta \cos(2\theta_B) + \beta\gamma \sin(2\theta_B)]$$

$$+ 2 \cos(2\theta_A) [\gamma\alpha + \gamma\beta \cos(2\theta_B) + \gamma\gamma \sin(2\theta_B)]$$

$$\equiv -2 \sin(2\theta_A) \mathcal{O}(\theta_B | \beta_A) + 2 \cos(2\theta_A) \mathcal{O}(\theta_B | \gamma_A) \quad (21)$$

And similar for $\mathcal{G}_B(\theta_A, \theta_B)$, by permutation of indices.

The Hessian is,

$$\mathcal{H}_{AA}(\theta_A, \theta_B) \equiv \frac{\partial^2 \mathcal{O}(\theta_A, \theta_B)}{\partial \theta_A^2}$$

$$= -4 \cos(2\theta_A) \mathcal{O}(\theta_B | \beta_A) - 4 \sin(2\theta_A) \mathcal{O}(\theta_B | \gamma_A) \quad (22)$$

And similar for $\mathcal{H}_{BB}(\theta_A, \theta_B)$, by permutation of indices, and,

$$\mathcal{H}_{AB}(\theta_A, \theta_B) \equiv \frac{\partial^2 \mathcal{O}(\theta_A, \theta_B)}{\partial \theta_A \partial \theta_B}$$

$$= -2 \sin(2\theta_A) \frac{\partial \mathcal{O}(\theta_B | \beta_A)}{\partial \theta_B} + 2 \cos(2\theta_A) \frac{\partial \mathcal{O}(\theta_B | \gamma_A)}{\partial \theta_B} \quad (23)$$

The stationary condition is,

$$\mathcal{G}_A(\theta_A, \theta_B) = 0$$

$$\Rightarrow \tan(2\theta_A) = \frac{\gamma\alpha + \gamma\beta \cos(2\theta_B) + \gamma\gamma \sin(2\theta_B)}{\beta\alpha + \beta\beta \cos(2\theta_B) + \beta\gamma \sin(2\theta_B)} \quad (24)$$

and,

$$\mathcal{G}_B(\theta_A, \theta_B) = 0$$

$$\Rightarrow \tan(2\theta_B) = \frac{\alpha\gamma + \beta\gamma \cos(2\theta_A) + \gamma\gamma \sin(2\theta_A)}{\alpha\beta + \beta\beta \cos(2\theta_A) + \gamma\beta \sin(2\theta_A)} \quad (25)$$

The minimal condition is,

$$\mathcal{H} \geq 0 \quad (26)$$

Note that this last expression means that the eigenspectrum of the Hessian should be positive at the stationary point to guarantee a local minimum. Also note that multiple local minima are sometimes present in the observables for ≥ 2 -gate tomography (we have empirically seen $1 \times$ or $2 \times$ local minima in 2-gate tomography).

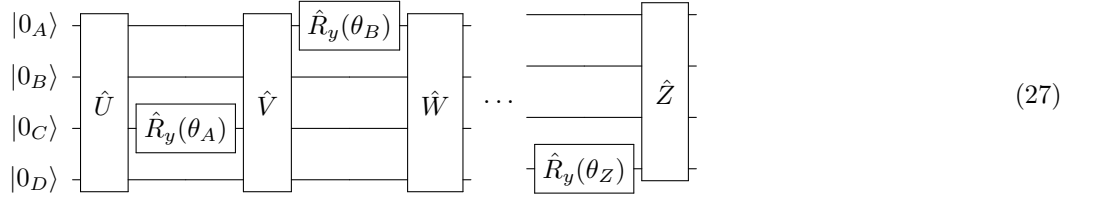
We have not, as yet, determined an analytical solution for the optimal angles θ_A and θ_B . However, after the tomography fitting has been performed, it is straightforward to classically optimize the angles to close to the machine precision on the analytical tomography surface. One particularly simple and robust procedure we have developed is to solve for the analytical optimal value of θ_A while θ_B is frozen (via applying the recipe of Equation 15 to Equation 24) and then to repeat to analytically optimize θ_B while θ_A is frozen. This procedure can be applied iteratively, and is guaranteed to converge monotonically toward a local minimum. We refer to this approach as the classical Jacobi-1 optimization approach (“1” for one single gate angle at a time). The monotonic convergence property makes the Jacobi optimization procedure particularly robust relative to gradient/Hessian-based methods such as Newton-Raphson or L-BFGS, which often fail or converge slowly for this objective function due to the indefinite or negative nature of the Hessian in large patches of the parameter space - a phenomenon for variational quantum observable expectation values that has previously been referred to as the “barren plateaus” issue.⁶⁴ Note that there are two caveats with the Ja-

cobi procedure: (1) the procedure may converge to spurious local minima and (2) the procedure converges rather slowly if there is high covariance of the observable expectation value $\mathcal{O}(\theta_A, \theta_B)$ with respect to the two parameters θ_A and θ_B . To combat (1), the classical tomography formula can be sampled with a medium-density rectilinear grid (e.g., a spacing of $\Delta\theta = \pi/8$) and the Jacobi-1 iteration seeded from the global minimum on the medium-density grid. To combat (2), one can switch to classical L-BFGS or full classical Newton-Raphson once the Jacobi optimization procedure has reached the neighborhood of a quadratic minimum.

A schematic of the 9-point quadrature and classical Jacobi-1 optimization procedure for two-gate tomography is depicted in Figure 3.

3. M -Gate Tomography

Now consider a general M - \hat{R}_y -gate quantum circuit of the form encountered in VQE,



The corresponding observable expectation value is,

$$\begin{aligned} \mathcal{O}(\theta_A, \theta_B, \dots, \theta_Z) \equiv \\ \langle 0 | \hat{U}^\dagger \hat{R}_y^\dagger(\theta_A) \hat{V}^\dagger \hat{R}_y^\dagger(\theta_B) \hat{W}^\dagger \dots \hat{R}_y^\dagger(\theta_Z) \hat{Z}^\dagger \\ \times \hat{Z} \hat{R}_y(\theta_Z) \dots \hat{W} \hat{R}_y(\theta_B) \hat{V} \hat{R}_y(\theta_A) \hat{U} | 0 \rangle \end{aligned} \quad (28)$$

Note that the alphabetical labeling $\theta_A, \theta_B, \dots, \theta_Z$ is merely illustrative - there can be more or less than 26 gates depending on M . This has the 3^M -parameter tomography,

$$\mathcal{O}(\theta_A, \theta_B, \dots, \theta_Z) = \sum_{\vec{I}} c_{\vec{I}} \prod_{i_D \in I} \phi_{i_D}(\theta_D)$$

Where \vec{I} ranges over the set of trinary strings of length M , e.g., 000, 001, 002, 010, 011, 012, 020, 021, 022, 100, etc, and the basis functions are $\phi_0(\theta) \equiv 1$, $\phi_1(\theta) \equiv \cos(2\theta)$, and $\phi_2(\theta) \equiv \sin(2\theta)$.

The tomography coefficients $\{c_{\vec{I}}\}$ can be computed from a 3^M -point quadrature grid consisting of a Cartesian grid of $\{-\pi/3, 0, +\pi/3\}$ in each angle. The transfer matrix is $\hat{T}_{(M)} \equiv \bigotimes_M \hat{T}_{(1)}$, and the corresponding inverse is $\hat{T}_{(M)}^{-1} \equiv \bigotimes_M \hat{T}_{(1)}^{-1}$.

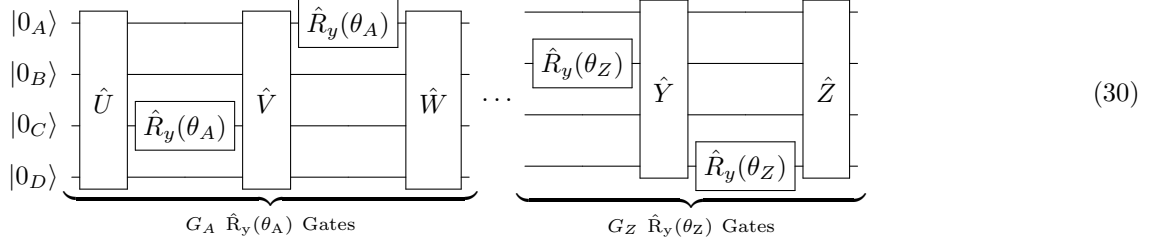
The gradient, Hessian, stationary conditions, and minimal conditions all follow straightforwardly from multi-dimensional extensions of Equations 21 to 26, e.g.,

$$\begin{aligned} \mathcal{G}_A(\theta_A, \theta_B, \dots, \theta_Z) &\equiv \frac{\partial \mathcal{O}(\theta_A, \theta_B, \dots, \theta_Z)}{\partial \theta_A} \\ &= -2 \sin(2\theta_A) \mathcal{O}(\theta_B, \dots, \theta_Z | \beta_A) \\ &\quad + 2 \cos(2\theta_A) \mathcal{O}(\theta_B, \dots, \theta_Z | \gamma_A) \end{aligned} \quad (29)$$

4. QAOA Tomography

In QAOA,² we often encounter a generalization/simplification where the angles of multiple \hat{R}_y gates

are pinned together. E.g., for an M -stage quantum circuit,



The corresponding observable expectation value is,

$$\begin{aligned} O(\theta_A, \dots, \theta_Z) \equiv \\ \langle 0 | \hat{U}^\dagger \hat{R}_y^\dagger(\theta_A) \hat{V}^\dagger \hat{R}_y^\dagger(\theta_A) \hat{W}^\dagger \dots \hat{R}_y^\dagger(\theta_Z) \hat{Y}^\dagger \hat{R}_y^\dagger(\theta_Z) \hat{Z}^\dagger \\ \times \hat{O} \hat{Z} \hat{R}_y(\theta_Z) \hat{Y} \hat{R}_y(\theta_Z) \dots \hat{W} \hat{R}_y(\theta_A) \hat{V} \hat{R}_y(\theta_A) \hat{U} | 0 \rangle \end{aligned} \quad (31)$$

This has the $\prod_D (2G_D + 1)$ -parameter tomography $[(2G + 1)^M$ if G_D is independent of D],

$$O(\theta_A, \dots, \theta_Z) = \sum_{\vec{I}} c_{\vec{I}} \prod_{i_D \in \vec{I}} \phi_{i_D}(\theta_D) \quad (32)$$

Where each digit of \vec{I} ranges from $-G_D$ to $+G_D$ (inclusive). The basis functions are $\sin(G_D \cdot 2\theta)$, \dots , $\sin(2 \cdot 2\theta)$, $\sin(1 \cdot 2\theta)$, 1 , $\cos(1 \cdot 2\theta)$, $\cos(2 \cdot 2\theta)$, \dots , $\cos(G_D \cdot 2\theta)$.

Two technical notes with the circuit above: (1) in QAOA, often the interstitial operators \hat{U} , \hat{V} , \dots are the identity, e.g., within commuting layers of 1-qubit driver terms and (2) above we have drawn the θ_A and θ_Z stages as disjoint, but they may be interleaved without changing the analysis.

For this case, a Cartesian product of $(2G_D + 1)$ -point Fourier grids is sufficient to resolve the tomography. The task is simply to redefine the grid, transfer matrix, and transfer matrix inverse. For general G_D , the Fourier grid is,

$$\theta_p = \frac{(p+1)\pi}{2G_D+1} - \frac{\pi}{2}, \quad p \in [0, 2G_D+1) \quad (33)$$

The transfer matrix is,

$$T_{ip}^G \equiv \phi_i(\theta_p) = \left[\frac{\sin(2i\theta_p)}{1} \right] \left[\cos(2i\theta_p) \right] \quad (34)$$

As before, the M -stage transfer matrix is $\hat{T}_{(M)} \equiv \bigotimes_D^M \hat{T}_{(1)}^{G_D}$, and the corresponding inverse is $\hat{T}_{(M)}^{-1} \equiv \bigotimes_D^M \hat{T}_{(1)}^{G_D, -1}$.

circuit, where each stage D has $G_D \hat{R}_y(\theta_D)$ gates,

The gradient and Hessian are easily computed along the lines of the approach used in the previous section, with specific partial derivatives of the basis functions $\phi_i(\theta_p)$.

An example Fourier quadrature resolution of a QAOA-type tomography function is depicted in Figure 4.

5. Tomography Formula Verification

The tomography formulae and quadrature recipes developed above were verified by dense Fourier grid comparison to randomly-generated quantum circuits (i.e., random \hat{O} and \hat{U} , \hat{V} , \dots) for up to $M = 5$ and up to to $G = 5$. All test cases exhibit a relative deviation between the analytical circuit simulation result and the quadrature-fitted tomography formula of $\sim 100\epsilon$, where $\epsilon \equiv 2.2 \times 10^{-16}$ is the double-precision machine epsilon, verifying that quadrature-based tomography fitting is analytical to close to the machine precision.

In closing this section, we make two observations regarding the Fourier quadrature resolution of the tomography parameters. The first observation is that the quadrature points are widely spaced in θ , and the tomography coefficients are resolved by the transfer matrix inverse with coefficients that are nearly unity. This means that roughly the same statistical convergence of the observable expectation value at each quadrature grid point is required to obtain a given absolute accuracy in the observable across the full tomography formula as is required to obtain the same absolute accuracy in the observable at a specific point. This is in marked contrast to, e.g., finite difference derivatives, where the observable must be resolved to much higher precision at the stencil grid points to obtain a given accuracy in the approximated derivative, due to subtractive cancellation. Since we are free to analytically differentiate the tomography formula, we obtain a recipe for the analytical gradient of the observable expectation which has the same number of required observable expectation value evaluations as the second-order symmetric finite difference formula, but with markedly reduced precision requirements. Tacitly,

for a single-gate example,

$$\mathcal{G}_A(\theta_A) \equiv \frac{\partial \mathcal{O}}{\partial \theta_A} = \frac{2}{\sqrt{3}} \mathcal{O}(\theta_A + \pi/3) - \frac{2}{\sqrt{3}} \mathcal{O}(\theta_A - \pi/3) \quad (35)$$

$$= \lim_{h \rightarrow 0} \left[\frac{1}{2h} \mathcal{O}(\theta_A + h) - \frac{1}{2h} \mathcal{O}(\theta_A - h) \right] \quad (36)$$

Here the top formula relies on the tomography formula resolved by Fourier quadrature, while the bottom formula uses the second-order symmetric finite difference formula. Both require $2P$ observable evaluations to compute the complete gradient for P gates, but the upper formula has markedly lower precision requirements at each grid point. Similar formulae occur for the Hessian and higher-order derivatives - in each case the number of required evaluations is the same as in second-order finite difference, but the wide spacing of the quadrature grid points reduce the precision requirements at each grid point. The only potential downside is that the computation of directional derivatives (i.e., the gradient projected along a given linear combination of circuit angles) requires the full $2P$ observable evaluations with the Fourier quadrature recipe, but generally requires $\mathcal{O}(1)$ observable evaluations with finite difference. The second observation is that the Fourier quadrature selected for the tomography fitting in this study is not the only valid choice of quadrature grid: any three distinct quadrature points would produce a non-singular transfer matrix that could analytically determine the tomography coefficients. For example, we have previously used the modified quadrature $\{-\pi/4, 0, +\pi/4\}$, and have also been able to resolve the analytical tomography formulae to $\sim 100\epsilon$, as expected. A final note is that a post-3-point quadrature (e.g., an E -point quadrature or a stochastic sampling along θ_A) might prove to be useful for error mitigation during tomography fitting on noisy quantum hardware. Here, additional information from the extended grid recipe could identify statistically significant differences from the expected tomography formula, which is definitionally noise and can be excluded by the extended tomography fitting.

B. Jacobi-Type Local Fixed-Point Iteration

At this point, the quadrature grid points, transformation to tomography coefficients, and characteristics such as gradients and Hessians can all be determined. What remains is to use these iterated partial tomography measurements to classically optimize VQE or QAOA quantum circuit parameters, as sketched in the middle panel of Figure 2. There seem to be many possible recipes involving maximum cluster size M , mixings of clusters of different sizes, cluster order, cluster order randomization, and consideration of circuit layout in selecting clusters and order. Here, we describe a few fairly obvious recipes,

Jacobi-1: All $M = 1$ single angles, in a definite order during each Jacobi sweep. This method requires a 3-point Fourier quadrature for the tomography at each angle, leading to $3P$ total observable evaluations for P gates (reducible $2P + 1$ if the central point of each quadrature is inferred from the tomography of the previous angle). This is complementary with the $2P$ observable evaluations required to compute the total circuit gradient in gradient-based methods, though note that the observations in gradient-based methods are parallelizable/pipelineable, while the observations in Jacobi-based measurements are usually serialized.

Jacobi-2: All $M = 2$ pairs of angle, in a definite order during each Jacobi sweep. This method requires a 9-point Fourier quadrature for the tomography at each angle pair, leading to $9P(P+1)/2$ total observable evaluations for P gates (prefactor reducible if the values at certain points are inferred from tomography fittings for other angles, in certain orders of angle pairs). This is complementary with the $4P(P+1)/2 + 2P + 1$ observable evaluations required to compute the total circuit Hessian for full Newton-Raphson-based optimization methods.

Jacobi-Gen: A generalized approach, with a user-specified sequence of clusters of angles is optimized in a given order. This requires 3^M observable evaluations for each M -gate cluster. The selection of such clusters is presently an art, but could be guided by considerations of spatial or temporal geometry within the quantum circuit, explicit computations to determine angle clusters with strong coupling, or other methods. The heuristic choice(s) selected for the numerical tests in the present manuscript are detailed below.

Jacobi-1-Rand: Jacobi-1, but with the order of angles shuffled randomly.

Jacobi-2-Rand: Jacobi-2, but with the order of angles shuffled randomly.

Jacobi-Gen-Rand: Jacobi-Gen, but with the order of angles shuffled randomly.

Many other possible Jacobi sweep recipes surely must exist - their determination is a worthy topic of future study.

C. Anderson-Type Global Convergence Acceleration

In practice, we have found that one additional step can sometimes substantially accelerate the global convergence of the Jacobi-type algorithm developed above,

at no additional cost (i.e., no additional quantum measurements, and very few classical operations): Anderson-type sequence acceleration. The Anderson method is arguably an unusual numerical methods technique that is often described as more of a recipe than an algorithm. It was developed by Anderson⁵¹ in 1965 as a pragmatic means of accelerating slowly-converging sequences, and was independently discovered as the direct inversion of the iterative subspace (DIIS) by Pulay⁵³ in 1980 (and furthered⁵⁴ in 1982) in the domain of electronic structure theory. Anderson acceleration resembles Krylov linear algebraic methods such as Lanczos, Arnoldi, GMRES, or Davidson-Liu, or the low-rank Hessian update quasi-Newton optimization methods such as Broyden, DFP, or L-BFGS in that it examines the iterative sequence and provides adjustive predictions to the sequence to accelerate convergence. However, the formal details of how Anderson acceleration works are mathematically rather murky - there are few guiding principles on how and why the method works, and this is an area of ongoing study. Part of the reason for this is that Anderson is actually a class of methods with many possible variations and applications. There have been several formal efforts that have shown that certain variations and applications of Anderson reduce to GMRES (for application to linear solutions),⁵² to Arnoldi iteration (for application to eigenstate solutions),⁵² or to a multi-secant-type method (for application to nonlinear root finding),⁶⁵ and have probed the formal convergence properties in those areas.

The basic idea of Anderson is, for a given set of nonlinear equations $f(\vec{\theta}) = 0$ (the “vector” symbol indicates the dimension of the parameter space), one is given an iterative sequence over iteration index i of state vectors $\vec{\theta}^i$ and error vectors $\vec{\epsilon}^i \equiv \vec{\theta}^i - \vec{\theta}$ so that $\vec{\theta}^i = \vec{\theta} + \vec{\epsilon}^i$. Anderson acceleration posits that at iteration k , an improved state vector $\vec{\theta}'^k$ can replace $\vec{\theta}^k$, and is composed of a linear combination of the current history of iterative state vectors,

$$\vec{\theta}'^k \equiv \sum_i c_i^k \vec{\theta}^i \quad (37)$$

The corresponding improved error vector is,

$$\vec{\epsilon}'^k \equiv \sum_i c_i^k \vec{\epsilon}^i \quad (38)$$

Anderson acceleration proposes that the coefficients c_i^k be chosen to minimize the square of the 2-norm of $\vec{\epsilon}'^k$,

$$O^k(c_i) = \sum_{ij} c_i^k c_j^k \vec{\epsilon}^i \cdot \vec{\epsilon}^j \quad (39)$$

subject to the normalization condition,

$$\sum_i c_i^k = 1 \quad (40)$$

In the limit of a sufficiently large iterative space to span the vector space for $\vec{\theta}$, this is guaranteed to produce the

desired result of $\theta'^k = \theta^k$, and will provide a least-squares error approximation in a less-complete limit. An analytical solution for the linearly-constrained least-squares problem is easily obtained,

$$\left[\begin{array}{ccc|c} B_{11} & \dots & B_{1k} & -1 \\ \vdots & \ddots & \vdots & \vdots \\ B_{k1} & \dots & B_{kk} & -1 \\ \hline -1 & \dots & -1 & 0 \end{array} \right] \left[\begin{array}{c} c_1^k \\ \vdots \\ c_k^k \\ \hline \lambda \end{array} \right] = \left[\begin{array}{c} 0 \\ \vdots \\ 0 \\ \hline -1 \end{array} \right] \quad (41)$$

Here $B_{ij} \equiv \vec{\epsilon}^i \cdot \vec{\epsilon}^j$ and λ is a Langrange multiplier corresponding to the normalization constraint. The numerical cost of predicting θ'^k from the iterative history is minimal (and all classical): only the inner-products in B_{ij} , a matrix inversion of the dimension of $k+1$, and the vector addition to form θ'^k are required.

The cognizant reader will have noticed that the above manipulations would all be for naught if we actually had the iterative history of the error vector $\vec{\epsilon}^k$: at any iteration (including the first iteration!), we could simply obtain the full solution as $\vec{\theta} = \vec{\theta}^k - \vec{\epsilon}^k$. In practice, Anderson acceleration replaces the iterative history of the exact error vector $\vec{\epsilon}^k$ with a proxy quantity $\tilde{\epsilon}^k$ that is pragmatically chosen to approximate a scaled error vector. For instance, the displacement of the parameters during a fixed-point iterative move $\delta\vec{\theta}^k \equiv \vec{\theta}^k - \vec{\theta}^{k-1}$ (the original Anderson⁵¹ and Pulay DIIS⁵³ proposals) may be effective slowly converging fixed-point series which are making large numbers of small moves in roughly the same direction (e.g., the convergence of the classical Jacobi-1 procedure for the $M = 2$ example in Figure 3). Alternatively, an approximately preconditioned gradient may prove more useful for accelerating nonlinear optimization procedures posed as gradient root finding or linear solve procedures posed as residual zero finding - this procedure was used in Pulay’s second DIIS paper in 1982,⁵⁴ and is industry standard for converging classical SCF equations.

Note that the invocation of Anderson or Pulay DIIS sequence acceleration techniques invalidate the monotonic convergence property of the Jacobi diagonalization-type procedure developed above. However, we note that Anderson/Pulay DIIS are robust methods - if a bad “move” is proposed, it will usually have a large associated error vector, and therefore its DIIS coefficient will be small.

1. Anderson-Style Acceleration

There are some implementation subtleties regarding the order of Jacobi and Anderson steps, the initiation of the iterative sequence, and the timing and history of the Anderson subspace. For Anderson-style acceleration, the explicit sequence is,

$$\vec{\theta}^0 \xrightarrow{\text{Jacobi}} \vec{\theta}^1 \xrightarrow{\text{DIIS}[\vec{\theta}^1, \delta\vec{\theta}^1 \equiv \vec{\theta}^1 - \vec{\theta}^0]} \quad (42)$$

$$\vec{\theta}^{*1} \xrightarrow{\text{Jacobi}} \vec{\theta}^{*2} \xrightarrow{\text{DIIS}[\vec{\theta}^{*2}, \delta\vec{\theta}^{*2} \equiv \vec{\theta}^{*2} - \vec{\theta}^{*1}]}$$

$$\begin{aligned} \vec{\theta}^2 \xrightarrow{\text{Jacobi}} \vec{\theta}^3 \xrightarrow{\text{DIIS}[\vec{\theta}^3, \delta\vec{\theta}^3 \equiv \vec{\theta}^3 - \vec{\theta}^2]} \\ \vdots \end{aligned}$$

Here $\text{DIIS}[\vec{\theta}, \vec{\epsilon}]$ is a subroutine call that adds state vector $\vec{\theta}$ and error vector $\vec{\epsilon}$ to the iterative history, and then returns an extrapolated result for $\vec{\theta}$ from the current contents of the iterative history.

2. Pulay-Style DIIS Acceleration

Similarly for Pulay-style DIIS as commonly implemented in SCF,

$$\vec{\theta}^0 \xrightarrow{\text{DIIS}[\vec{\theta}^0, \vec{G}(\theta^0)]} \vec{\theta}^1 \xrightarrow{\text{Jacobi}} \quad (43)$$

$$\vec{\theta}^1 \xrightarrow{\text{DIIS}[\vec{\theta}^1, \vec{G}(\theta^1)]} \vec{\theta}^2 \xrightarrow{\text{Jacobi}}$$

$$\vec{\theta}^2 \xrightarrow{\text{DIIS}[\vec{\theta}^2, \vec{G}(\theta^2)]} \vec{\theta}^3 \xrightarrow{\text{Jacobi}}$$

\vdots

Here $\vec{G}(\vec{\theta})$ is the gradient vector $\frac{\partial \mathcal{O}}{\partial \theta_g}$ at the current parameter set. With some minimal logical statements, these can be written in one monolithic Jacobi+Anderson code.

D. Relationship with Powell's Method

Consideration of the methods developed above with existing classical optimization algorithms reveals an interesting comparison of the Jacobi-1 method with a closely related algorithm: Powell's gradient-free optimization method.⁶² Each iteration of Powell's method involves sweeping over a set of search directions (a set of generally non-orthogonal normal vectors in the parameter space, with the set dimension being equal to the number of parameters) and sequentially performing a bidirectional linesearch along each search direction to find a local minimum. At the end of each iteration, the total displacement of the iteration is added as a new search direction, and the previous search direction that contributed the most to the total displacement over the iteration is discarded. The first iteration of Powell and Jacobi-1 are identical if the standard normal vectors in the basis of circuit parameters are used as the initial search directions for Powell. Subsequently, Powell is able to avoid the convergence stagnation that will be observed shortly for DIIS-free Jacobi-1 by searching along directions that are linear combinations of multiple circuit parameters (whereas

Jacobi-1 is always constrained to search along only individual circuit parameters). The penalty for the flexibility of Powell is that a bidirectional linesearch must be performed along each search direction, generally requiring a modest number ($\sim 12 - 14$) of observable expectation values for each search direction.

Jacobi-1 augmented with Anderson or Pulay DIIS might offer a method that is correspondent and competitive with Powell: here, the number of observables per Jacobi-1 iteration is strictly $3M$ ($2M + 1$ with tomography formula reuse), and the raw Jacobi-1 constraint to rectilinear search directions along circuit single circuit parameters is mitigated by the DIIS extrapolation, allowing one to move "diagonally" through the parameter space. Below we will see that the early convergence history of Jacobi-1-Anderson and Jacobi-1-DIIS are remarkably similar to Powell, though the latter method requires several times more observables per iteration to carry out linesearches.

III. COMPUTATIONAL DETAILS

The Fourier quadrature grid based tomography fitting procedure and Jacobi+Anderson optimization algorithms were implemented for MC-VQE in our in-house quantum simulator package QUASAR. For the purposes of this study, noise channels and statistical errors are not modeled: the observable expectation values are computed by double-precision contraction of the simulated qubit wavefunctions to the relevant Pauli density matrices. This directly probes the characteristics of the algorithms in the absence of noise, allowing for analysis of both the initial convergence behavior (in the statistical and NISQ-limited hardware regime) and the terminal/global convergence behavior (in the tightly-converged limit, relevant for classical benchmarking). Future studies will investigate the robustness of these algorithms under statistical and device noise channels, on simulated and physical hardware.

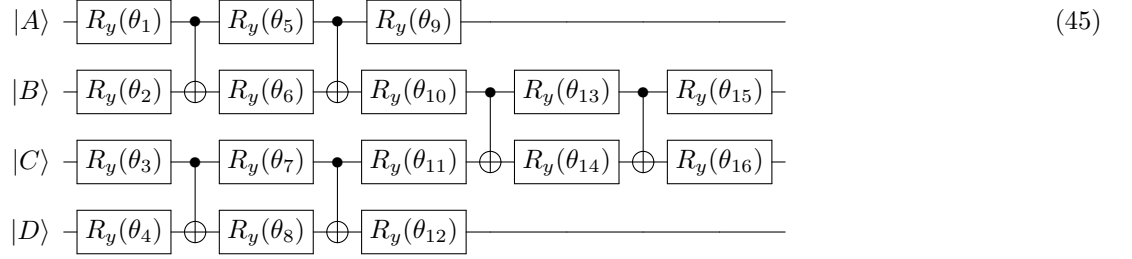
To demonstrate the characteristics of the involved algorithms, we have selected an "easy" and "hard" VQE optimization test case from our recently-developed MC-VQE+AIEM methodology. In both cases, we consider an $N = 4$ monomer/qubit system of a linearly arranged set of chromophores from the B850 ring of LHII (the first four chromophores from the $N = 18$ example of the MC-VQE theory paper, with nearest neighbor linear connectivity and dipole-dipole couplings). In all cases, we prepare a number N_Θ of "contracted reference states," $|\Phi_\Xi\rangle \equiv \sum_r C_{r\Xi} |\vec{I}\rangle$ taken here from classical configuration interaction singles (CIS) with restricted configurations $|\vec{I}\rangle$ including the reference configuration $|0000\rangle$ and all singly-excited configurations, e.g., $|0010\rangle$. A simple quantum circuit to prepare such states was shown in our MC-VQE paper. These are then correlated with a VQE entangler circuit $\hat{U}(\{\theta_g\})$ so as to minimize the expecta-

tion value of the state-averaged energy,

$$\mathcal{O}(\{\theta_g\}) \equiv \frac{1}{N_\Theta} \sum_{\Xi} \langle \Phi_{\Xi} | \hat{U}^\dagger(\{\theta_g\}) \hat{H} \hat{U}(\{\theta_g\}) | \Phi_{\Xi} \rangle \quad (44)$$

Subsequent to state-averaged VQE optimization, the contracted subspace Hamiltonian

$H_{\Xi\Xi'} \equiv \langle \Phi_{\Xi} | \hat{U}^\dagger(\{\theta_g\}) \hat{H} \hat{U}(\{\theta_g\}) | \Phi_{\Xi'} \rangle$ can be computed by additional quantum measurements, then classically diagonalized to form the adiabatic MC-VQE states $|\Psi_\Theta\rangle$ and corresponding diagonal or transition properties. The selected state-averaged VQE entangler circuit is,



Note the lexical ordering of $N_g = 16$ gate angles, arbitrarily chosen to run with the qubit index fast and the time index slow.

The origins of the “easy” and “hard” test cases come from the consideration of the dense spectrum of the excited states $|\Psi_1\rangle$ to $|\Psi_5\rangle$ - under the exact full configuration interaction (FCI) solution, these lie between 1.84 and 2.10 eV above the ground state, and have markedly different oscillator strengths. The “easy” test case is chosen by selecting $N_\Theta = 5$ - here, the specifics of the CIS contracted reference states are not important, as the whole singles manifold is covered. In this case, the goal of the state-averaged VQE entangler circuit is to decouple the ground and first four excited states (dominated by linear combinations of single excitations) from the rest of the Hilbert space - the subsequent subspace diagonalization procedure will handle rotations within the entangled contracted reference states to form the final MC-VQE adiabatic states. The “hard” test case is chosen by selecting $N_\Theta = 3$ - here, the state-averaged VQE entangler circuit must also decouple the target states from states $|\Psi_4\rangle$ and $|\Psi_5\rangle$, involving considerable singles-singles mixing. This is analogous to targeting a subset of densely packed eigenstates in classical linear algebra algorithms, which is known to cause slow convergence in methods such as Lanczos, or Davidson-Liu. In practice, we find that the “hard” case is generally much more difficult to converge to any given local minimum than the “easy” case, exhibits more significantly multiple local minima than we observe in the “easy” case, and has higher errors for absolute and difference energies and transition properties than the “easy” case, regardless of which local minimum is converged.

In the numerical tests, we compare the standard L-BFGS and Powell implementations in SCIPY to various Jacobi methods. For the Jacobi methods, we consider

the standard “Jacobi-1” [all single angle pivots (θ_g, \cdot) , in lexical order] and “Jacobi-2” [all double angle pivots $(\theta_g, \theta'_g) : g \geq g'$]. We also explore the use of the generalized Jacobi recipe by considering two variants of sieved Jacobi-2: “Jacobi-A,” in which all two-angle pivots on the same qubit index are included [e.g., (θ_5, θ_1) , (θ_9, θ_1) , and (θ_9, θ_5) , but not (θ_2, θ_1) or (θ_3, θ_1)], and “Jacobi-B,” in which all two-angle pivots on linearly adjacent qubit indices are included [e.g., adding (θ_2, θ_1) but not (θ_3, θ_1) to the Jacobi-A example]. For this example, Jacobi-1 requires 3-point tomography of 16 gates, for 48 total observables per iteration (reducible to 33 observables per iteration if tomography information is reused between gate optimizations). Jacobi-2 requires 9-point tomography of 120 gate pairs, for 1080 total observables per iteration. Jacobi-A requires 9-point tomography of 26 gate pairs, for 234 total observables per iteration. Jacobi-B requires 9-point tomography of 81 gate pairs, for 729 total observables per iteration. Gradient-based methods like L-BFGS require 33 at least observables per iteration: for L-BFGS we find typically ~ 36 observables per iteration, with line searches to updated trust regions. Powell requires a line search per gate per iteration: we find typically ~ 220 observables per iteration.

We also explore various convergence acceleration approaches. One possibility is to randomize the pivot order of the standard Jacobi procedure, a method denoted “Jacobi- F -Random.” We also use Anderson acceleration applied with the traditional Anderson error vector of the move length $\{\delta\theta'_g\}^k$ (“Jacobi- F -Anderson”) and with the Pulay DIIS error vector of the energy gradient $\{\frac{\partial \mathcal{O}}{\partial \theta_g}\}^k$ (“Jacobi- F -Pulay”). The second choice additionally requires the computation of the gradient after each Jacobi sweep, bringing the total number of observables per iteration to 81. For the DIIS procedure, we store at most 10

iterative history vectors with a worst-error removal policy, and we flush the DIIS iterative history every 40 iterations. We have tested mixing pivot randomization and Anderson/Pulay variants of DIIS, and have found (as expected) that the DIIS procedure cannot tolerate the randomized pivots and does not provide any improvement over Jacobi-Random. Therefore, we do not explicitly discuss mixings of Jacobi-Rand and Jacobi-Anderson/Pulay below.

In all cases, we start from a guess of zero entanglement $\{\theta_g = 0\}$. We converge each algorithm for 100 iterations or until a maximum gradient element in the state-averaged energy falls below 1×10^{-7} .

IV. RESULTS AND DISCUSSION

Including the classes of Jacobi-1, Jacobi-2, Jacobi-A, and Jacobi-B and their direct product with the choices of no convergence acceleration, pivot randomization, Anderson, and Pulay, plus the reference L-BFGS and Powell methods, there are $18 \times$ optimization methods to test. To proceed, we will compare the convergence of different methods within a given Jacobi class (wherein logical iterations for the various convergence acceleration methods all cost the same number of observable expectation values, up to the additional modest gradient evaluation cost of Pulay), to downselect the convergence acceleration method to one case per Jacobi class. We will then compare the different selected Jacobi methods to each other and to L-BFGS and Powell first with respect to logical iteration count, and finally with respect to convergence as a function of number of observable expectation values. The latter is the ultimate cost function: optimization of variational quantum circuits within the statistical and device noise limit on near-term quantum hardware requires optimization algorithms with rapid initial convergence relative to the number of required observable expectation values, while classical benchmark testing requires optimization algorithms with fast and robust global convergence relative to the number of required observable expectation values.

A. Jacobi-1 Methods (All Single Angles)

Figure 5 shows the convergence of the Jacobi-1 methods for the N_{state} “easy” test case. The first finding is that a single iteration of Jacobi-1 can provide a relatively good starting point that is substantially lower in energy and maximum gradient than the result of the first logical L-BFGS iteration (not visible in the energy figure), and identical in quality to the first logical Powell step. The latter observation is expected: the first step of Jacobi-1 and Powell are identical in spirit, though the Jacobi-1 recipe has an analytical 3-point formula that yields and exact linesearch. The second finding is that the unaccelerated Jacobi-1 methods experience rapid conver-

gence stagnation for these types of variational quantum circuits. This is indicated by the slow monotonic decay of the energy for Jacobi-1 and Jacobi-1-Random. A third finding is that pivot randomization seems to have substantial effect on the quality of the first iteration, but does not affect the convergence stagnation (emphasis that the pivots are randomized in every logical iteration). This indicates that other choices of deterministic Jacobi-1 pivot order should be explored to achieve the best initial iteration, but also indicates that pivot randomization should not be pursued. A fourth finding is that Jacobi-1-Anderson, Jacobi-1-Pulay, and Powell all perform remarkably similarly during the first part of the iterative procedure: all rapidly settle near a fixed point that appears to be associated with a saddle point or local minimum for a few iterations, and then all turn over at iteration 4 or 5 and converge rapidly toward the presumed global minimum. This indicates that the Anderson or Pulay convergence acceleration procedures can be successful at analyzing the iterative histories of moves and moving “diagonally” across the parameter space to target deeper minima and enhance convergence. The correspondence of this turnover with that of Powell is striking, particularly because Jacobi-1-Anderson/Pulay and Powell are operating by different mechanisms (and the Jacobi-1-Anderson/Pulay methods are several times cheaper than Powell due to the ability to forgo a linesearch for each search direction). The final finding is that the Anderson/Powell iterations do exhibit some oscillation in the terminal convergence epoch (particularly as the DIIS iterative history is flushed every 10 iterations), and end up stagnating at a maximum gradient element of $\sim 10^{-7}$. Powell seems to be more robust for extremely tight convergence - to mitigate this behavior, we can either develop methods to dampen the DIIS flushes, add characteristics to the DIIS iterative history to penalize for increased energy during the iterations as is done in the EDIIS extension,⁵⁹ or simply switch to Powell in the later stages of very tight classical optimizations needed for benchmarking variational quantum circuits.

Figure 6 shows the convergence of the Jacobi-1 methods for the N_{state} “hard” test case. The findings for this case are broadly similar as for the “easy” test case: the rapid early start relative to L-BFGS, expected stagnation of Jacobi-1 and Jacobi-1-Random, and remarkable correspondence of Jacobi-1-Anderson/Pulay to Powell continue. The primary difference in this case is the appearance of multiple stagnation points in the more-complicated objective function landscape for the hard problem. Though the Jacobi-1-Anderson/Pulay methods initially follow the Powell method, in later methods they slow down and more-closely follow the L-BFGS convergence. Powell remains the most robust method shown for tight convergence, and produces a markedly lower energy than predicted by any Jacobi-1 or L-BFGS method for this hard test case, albeit with several times more objective function evaluations per logical iteration.

For the global comparison below, we select the Jacobi-

1-Pulay method for the Jacobi-1 class, as it exhibits fewer/smaller oscillations near DIIS restarts. However, we reiterate that improving the overall monotonicity of the DIIS procedure is certainly a worthy topic for future study.

B. Jacobi-2 Methods (All Pairs of Angles)

Figure 7 shows the convergence of the Jacobi-2 methods for the N_{state} “easy” test case. The first finding is that the result after the first logical iteration of Jacobi-2 is substantially lower in energy and maximum gradient element than for Powell or the previously considered Jacobi-1, albeit at substantially higher cost in terms of require number of observable expectation values. The second finding is that pivot randomization does not improve convergence, as expected. The third finding is that neither Anderson nor Pulay convergence acceleration appear to offer significant improvement over the natural fixed-point convergence of Jacobi-2. This is not unexpected given the strong relationship of DIIS to second-order quasi-Newton methods, together with the fact that Jacobi-2 is using information equivalent to the full Hessian - it is likely that the natural second-order aspect of Jacobi-2 is redundant with the approximate second-order DIIS procedure. The last finding is that the convergence of Jacobi-2 stagnates at a maximum gradient element of $\sim 10^{-2}$, while the Powell method is immune to this problem - as before, Powell is superior for very tightly converged optimizations.

Figure 8 shows the convergence of the Jacobi-2 methods for the N_{state} “hard” test case. The results are similar to the easy case, with a few caveats. The first is that the starting point and convergence rate of Jacobi-1 are somewhat worse than the easy case. The second is that while the Pulay variant of DIIS seems to provide some improvement in energy convergence of Jacobi-2, the Jacobi-2-Anderson method exhibits an energy oscillation during the DIIS flush procedure at the 10th iteration. and then converges to a different, higher local minimum.

For the global comparison below, we select the Jacobi-2 method for the Jacobi-2 class, due to the apparent redundancy between the second-order aspects of Jacobi-2 and the approximate second-order DIIS method.

C. Jacobi-A Methods (All Pairs of Angles Within Single Qubit Wires)

Figures 9 and 10 show the convergence of the Jacobi-A methods for the N_{state} “easy” and “hard” test cases, respectively. The results from the Jacobi-A methods are remarkably similar to those from the Jacobi-2 methods, despite the angle pairs being restricted to be within individual qubit wires for Jacobi-A. Also worth noting is that the Jacobi-A-Pulay method exhibits a similar energy oscillation during the DIIS flush procedure and convergence

to a different local minimum, similar as was seen for this test case in Jacobi-2-Anderson. This indicates that the energy oscillations and subsequently problematic convergence with DIIS acceleration in Jacobi-2 methods is not specific to the choice of Anderson or Pulay error vectors. As with Jacobi-2, we select the unaccelerated Jacobi-A method for the global comparison below.

D. Jacobi-B Methods (All Pairs of Angles Within Single and On Adjacent Qubit Wires)

Figures 11 and 12 show the convergence of the Jacobi-A methods for the $N_{\text{state}} = 5$ and 3, “easy” and “hard” test cases, respectively. The results are entirely congruent with the findings for the Jacobi-2 and Jacobi-A methods above, which is not surprising as the angle pair constituents of Jacobi-B fall between Jacobi-2 and Jacobi-A. As with Jacobi-2 or Jacobi-A, we select the unaccelerated Jacobi-B method for the global comparison below.

E. Global Optimization Method Comparison vs. Logical Iteration Number

Figure 13 shows the convergence of the selected Jacobi methods and the L-BFGS and Powell methods for the $N_{\text{state}} = 5$ “easy” test case. The results show that Jacobi-1-Pulay and Powell have a highly similar convergence history, though the Jacobi-1-Pulay method is several times cheaper. Both Jacobi-1-Pulay and Powell exhibit faster logical convergence than L-BFGS. Jacobi-A, Jacobi-B, and Jacobi-2 all exhibit even more improved initial iterations, and converge logically faster than the other methods, but cost considerably more observable expectation values per iteration. The Jacobi methods all stagnate at a maximum gradient element of $\sim 10^{-7}$, while the Powell method eventually drops below this value - therefore Powell’s method remains superior for extremely tightly converged optimizations. A final note is the correspondence between Jacobi-A/B/2: all three are similar, while Jacobi-B and Jacobi-2 are essentially coincident.

Figure 14 shows the convergence of the selected Jacobi methods and the L-BFGS and Powell methods for the $N_{\text{state}} = 3$ “hard” test case. The results are similar to those for the “easy” test case, with the exception that the starting points and convergence rates are somewhat worse for all methods, and that the Jacobi-1-Pulay method starts out coincident with the logical iteration progress of Powell, but eventually degrades to be more coincident with L-BFGS.

F. Global Optimization Method Comparison vs. Observable Expectation Value Count

For deployment of variational quantum algorithms on near-term hardware, a key challenge is to minimize the

number of observables expectation values that must be statistically resolved to optimize the circuit parameters. In Figure 15, we compare the early convergence history of the selected Jacobi methods with L-BFGS and Powell for the “easy” test case. Here the overhead of bidirectional linesearch in Powell becomes apparent: the early convergence history of Jacobi-1-Pulay and Power are highly similar, but the Powell curve is scaled by a factor of ~ 2.6 . Jacobi-1-Pulay achieves early gains over L-BFGS, but becomes nearly coincident with L-BFGS as the optimization progresses. Note that there would be an additional gain if Jacobi-1-Anderson were plotted here due to the reduced overhead from the computation of the gradient needed for the Jacobi-1-Pulay error vector, but we did not select Jacobi-1-Anderson due to oscillations present in the DIIS flush procedure in later iterations. The Jacobi-A method is also notable: its first iteration achieves a high accurate-to-cost-ratio starting point that is well below the false minimum seen in the first few iterations of Jacobi-1-Pulay and Powell. Variations on Jacobi-A might prove useful to provide robust but low cost initial starting points near the global minimum.

In Figure 16, we compare the early convergence history of the selected Jacobi methods with L-BFGS and Powell for the “hard” test case. Here, the Jacobi-1-Pulay method retains the prefactor gain over Powell, but the convergence profile closely resembles L-BFGS. We again point out that we could improve matters by removing the gradient computation overhead in Jacobi-1-Pulay by switching to Anderson, if the DIIS flush procedure of Anderson could be stabilized. We also see the same substantial early-iteration gains for Jacobi-A as seen for the easy test case.

Overall, we observe that Jacobi-1-Pulay has an early convergence history that is several times faster than Powell and never worse than L-BFGS, and we observe that Jacobi-A provides the lowest-cost route to a robust starting point.

V. SUMMARY AND OUTLOOK

We have introduced and numerically explored a general class of methods for variational quantum circuit optimization based on Jacobi-diagonalization-type sweeps over fully converged sub-optimizations of localized clusters of circuit parameters. Evaluation of the observable expectation value at small Fourier quadrature grids allows for the tomography of the observable to be fit to a simple analytical form, allowing for offline classical optimization over the free parameters in each cluster. Various cluster strategies are proposed, including all single angles (Jacobi-1), all pairs of angles (Jacobi-2), and qubit-locality-based restrictions thereof (Jacobi-A and Jacobi-B). We also investigated the augmentation of the Jacobi method with Anderson acceleration through either the traditional Anderson recipe or the Pulay DIIS recipe. We numerically tested the Jacobi+Anderson methods

against the closely-related gradient-free Powell method and the gradient-based L-BFGS method for a pair of test cases taken from our MC-VQE+AIEM methodology. Jacobi-1-Pulay was found to provide an early convergence history that is identical to but several times faster than Powell, with regard to the number of observable expectation values required. The early convergence history of Jacobi-1-Pulay is competitive with and sometimes faster than L-BFGS. Jacobi-A was found to provide an initial iteration with remarkably low error at correspondingly low cost in terms of number of observable expectation values required, and may prove highly useful as a robust starting point that avoids many higher-lying local minima.

A number of outstanding technical developments remain to be done that might serve to make the methodology even more useful. Heuristics or guidelines for the selection of a more-optimal Jacobi sweep pivot order might provide enhanced convergence rates within each class of Jacobi method. A thorough exploration of the sieving of insignificant Jacobi-2 pairs to produce alternatives to Jacobi-A or Jacobi-B might produce additional approaches with costs similar to Jacobi-1 but convergence rates closer to Jacobi-2. It is also worth considering the addition of certain key 3- and 4-parameter clusters, which are more expensive to individually optimize, but might drastically improve global convergence. With regard to the Anderson and Pulay DIIS convergence acceleration explored here, it is worth considering other pairings of state and error vectors. It is also necessary to pursue extensions such as EDIIS⁵⁹ that penalize non-monotonic convergence behavior and to stabilize the DIIS flush procedure.

Further afield, it appears that the methodology introduced here is likely just one of many possible developments in optimization techniques that could make progress by consideration of the unique mathematical form and constraints of the optimization problem in variational quantum circuit algorithms. For instance, the constraint that the tomography is easier to resolve along individual circuit angles than in arbitrary search directions was the main motivation for the development of Jacobi-1-Anderson and Jacobi-1-Pulay. It is plausible that similar knowledge could be used to lower the cost of the linesearch in Powell’s method. In another direction, one could also consider the use of non-quadrature-based tomography fitting within the Jacobi steps, which might prove to be more resilient to device noise channels. In any case, the introduction of Jacobi fixed-point iteration and Anderson/Pulay DIIS acceleration techniques provides a promising new direction to explore to meet the challenge of optimizing variational quantum circuits on NISQ-era quantum hardware.

Note Added in Proof: While finalizing our manuscript, we became aware of similar work by Nakanishi, Fujii, and Todo, which was posted on the arXiv very recently.⁶⁶ The technical derivations in their manuscript cover many of the same topics and findings as we do,

and Nakanishi et al. numerically demonstrate an optimization method that appears to be very similar to one of the methods we describe, Jacobi-1.

Acknowledgements: R.M.P. thanks Dr. Edward G. Hohenstein, Prof. Todd J. Martínez, and Prof. C. David

Sherrill for years of discussions on Jacobi- and DIIS-type methods for classical electronic structure theory.

Conflict of Interest Disclosure: R.M.P., J.T.I., A.O., and P.L.M. hold stock/options in QC Ware Corporation.

-
- * Electronic address: rob.parrish@qcware.com
- ¹ A. Peruzzo et al., Nat. Comm. **5**, 4213 (2014).
 - ² E. Farhi, J. Goldstone, and S. Gutmann, arXiv preprint arXiv:1411.4028 (2014).
 - ³ J. Preskill, Quantum **2**, 79 (2018).
 - ⁴ J. R. McClean, J. Romero, R. Babbush, and A. Aspuru-Guzik, New J. Phys. **18**, 023023 (2016).
 - ⁵ P. OMalley et al., Phys. Rev. X **6**, 031007 (2016).
 - ⁶ A. Kandala et al., Nature **549**, 242 (2017).
 - ⁷ J. R. McClean et al., arXiv preprint arXiv:1710.07629 (2017).
 - ⁸ J. Romero et al., Quant. Sci. Tech. **4**, 014008 (2018).
 - ⁹ O. Higgott, D. Wang, and S. Brierley, arXiv preprint arXiv:1805.08138 (2018).
 - ¹⁰ J. Lee, W. J. Huggins, M. Head-Gordon, and K. B. Whaley, J. Chem. Theory Comput. (2018).
 - ¹¹ J. R. McClean, M. E. Kimchi-Schwartz, J. Carter, and W. A. de Jong, Phys. Rev. A **95**, 042308 (2017).
 - ¹² J. I. Colless et al., Phys. Rev. X **8**, 011021 (2018).
 - ¹³ K. M. Nakanishi, K. Mitarai, and K. Fujii, arXiv preprint arXiv:1810.09434 (2018).
 - ¹⁴ R. M. Parrish, E. G. Hohenstein, P. L. McMahon, and T. J. Martinez, arXiv preprint arXiv:1901.01234 (2019).
 - ¹⁵ T. Takeshita et al., arXiv preprint arXiv:1902.10679 (2019).
 - ¹⁶ Y. Nam et al., arXiv preprint arXiv:1902.10171 (2019).
 - ¹⁷ A. Lucas, Frontiers in Physics **2**, 5 (2014).
 - ¹⁸ F. Glover and G. Kochenberger, arXiv preprint arXiv:1811.11538 (2018).
 - ¹⁹ S. Hadfield et al., Algorithms **12**, 34 (2019).
 - ²⁰ V. N. Smelyanskiy et al., arXiv preprint arXiv:1204.2821 (2012).
 - ²¹ R. Biswas et al., Parallel Computing **64**, 81 (2017).
 - ²² R. Orús, S. Mugel, and E. Lizaso, Reviews in Physics , 100028 (2019).
 - ²³ E. Farhi, J. Goldstone, S. Gutmann, and H. Neven, arXiv preprint arXiv:1703.06199 (2017).
 - ²⁴ J. Otterbach et al., arXiv preprint arXiv:1712.05771 (2017).
 - ²⁵ N. Moll et al., Quantum Science and Technology **3**, 030503 (2018).
 - ²⁶ A. Gilyén, S. Arunachalam, and N. Wiebe, Optimizing quantum optimization algorithms via faster quantum gradient computation, in *Proceedings of the Thirtieth Annual ACM-SIAM Symposium on Discrete Algorithms*, pages 1425–1444, SIAM, 2019.
 - ²⁷ G. E. Crooks, arXiv preprint arXiv:1811.08419 (2018).
 - ²⁸ L. Zhou, S.-T. Wang, S. Choi, H. Pichler, and M. D. Lukin, arXiv preprint arXiv:1812.01041 (2018).
 - ²⁹ F. G. Brandao, M. Broughton, E. Farhi, S. Gutmann, and H. Neven, arXiv preprint arXiv:1812.04170 (2018).
 - ³⁰ G. Nannicini, Physical Review E **99**, 013304 (2019).
 - ³¹ G. G. Guerreschi and M. Smelyanskiy, arXiv preprint arXiv:1701.01450 (2017).
 - ³² J. Li, X. Yang, X. Peng, and C.-P. Sun, Physical Review Letters **118**, 150503 (2017).
 - ³³ K. Mitarai, M. Negoro, M. Kitagawa, and K. Fujii, Physical Review A **98**, 032309 (2018).
 - ³⁴ G. Verdon, J. Pye, and M. Broughton, arXiv preprint arXiv:1806.09729 (2018).
 - ³⁵ V. Bergholm, J. Izaac, M. Schuld, C. Gogolin, and N. Kil-loran, arXiv preprint arXiv:1811.04968 (2018).
 - ³⁶ M. Schuld, V. Bergholm, C. Gogolin, J. Izaac, and N. Kil-loran, Physical Review A **99**, 032331 (2019).
 - ³⁷ J. R. McClean, S. Boixo, V. N. Smelyanskiy, R. Babbush, and H. Neven, Nature communications **9**, 4812 (2018).
 - ³⁸ C. G. J. Jacobi, J. Reine Angew. Math. , 51 (1846).
 - ³⁹ A. H. Karp and J. Greenstadt, Parallel Computing **5**, 281 (1987).
 - ⁴⁰ G. H. Golub and H. A. van der Vorst, J. Comp. Appl. Math. **123**, 35 (2000), Numerical Analysis 2000. Vol. III: Linear Algebra.
 - ⁴¹ A. Bunse-Gerstner, R. Byers, and V. Mehrmann, SIAM J. Mat. Anal. Appl. **14**, 927 (1993).
 - ⁴² J.-F. Cardoso and A. Souloumiac, SIAM J. Mat. Anal. Appl. **17**, 161 (1996).
 - ⁴³ S. F. Boys, Rev. Mod. Phys. **32**, 296 (1960).
 - ⁴⁴ C. Edmiston and K. Ruedenberg, Rev. Mod. Phys. **35**, 457 (1963).
 - ⁴⁵ J. Pipek and P. G. Mezey, J. Chem. Phys. **90**, 4916 (1989).
 - ⁴⁶ G. Knizia, J. Chem. Theory Comput. **9**, 4834 (2013).
 - ⁴⁷ R. Dawes and T. Carrington, J. Chem. Phys. **121**, 726 (2004).
 - ⁴⁸ R. Dawes and T. Carrington, J. Chem. Phys. **122**, 134101 (2005).
 - ⁴⁹ R. Dawes and T. Carrington, J. Chem. Phys. **124**, 054102 (2006).
 - ⁵⁰ R. M. Parrish, E. G. Hohenstein, T. J. Martínez, and C. D. Sherrill, J. Chem. Phys. **138**, 194107 (2013).
 - ⁵¹ D. G. Anderson, J. ACM **12**, 547 (1965).
 - ⁵² H. F. Walker and P. Ni, SIAM J. Num. Anal. **49**, 1715 (2011).
 - ⁵³ P. Pulay, Chem. Phys. Lett. **73**, 393 (1980).
 - ⁵⁴ P. Pulay, J. Comp. Chem. **3**, 556 (1982).
 - ⁵⁵ T. P. Hamilton and P. Pulay, J. Chem. Phys. **84**, 5728 (1986).
 - ⁵⁶ J. Hutter, H. P. Lüthi, and M. Parrinello, Comp. Mat. Sci. **2**, 244 (1994).
 - ⁵⁷ G. E. Scuseria, T. J. Lee, and H. F. Schaefer III, Chem. Phys. Lett. **130**, 236 (1986).
 - ⁵⁸ P. Császár and P. Pulay, J. Mol. Struct. **114**, 31 (1984).
 - ⁵⁹ K. N. Kudin, G. E. Scuseria, and E. Cancès, J. Chem. Phys. **116**, 8255 (2002).
 - ⁶⁰ Y. K. Chen and Y. A. Wang, J. Chem. Theory Comput. **7**, 3045 (2011).
 - ⁶¹ W. Hu, L. Lin, and C. Yang, J. Chem. Theory Comput. **13**, 5458 (2017).
 - ⁶² M. J. Powell, Comp. J. **7**, 155 (1964).

- ⁶³ R. H. Byrd, P. Lu, J. Nocedal, and C. Zhu, SIAM Journal on Scientific Computing **16**, 1190 (1995).
- ⁶⁴ J. R. McClean, S. Boixo, V. N. Smelyanskiy, R. Babbush, and H. Neven, arXiv preprint arXiv:1803.11173 (2018).
- ⁶⁵ H.-r. Fang and Y. Saad, Numerical Linear Algebra with Applications **16**, 197 (2009).
- ⁶⁶ K. M. Nakanishi, K. Fujii, and S. Todo, arXiv preprint arXiv:1903.12166 (2019).

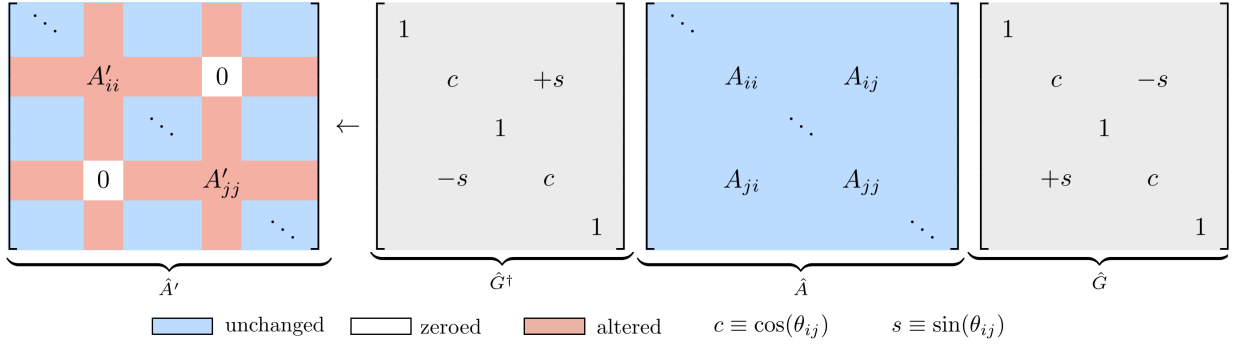
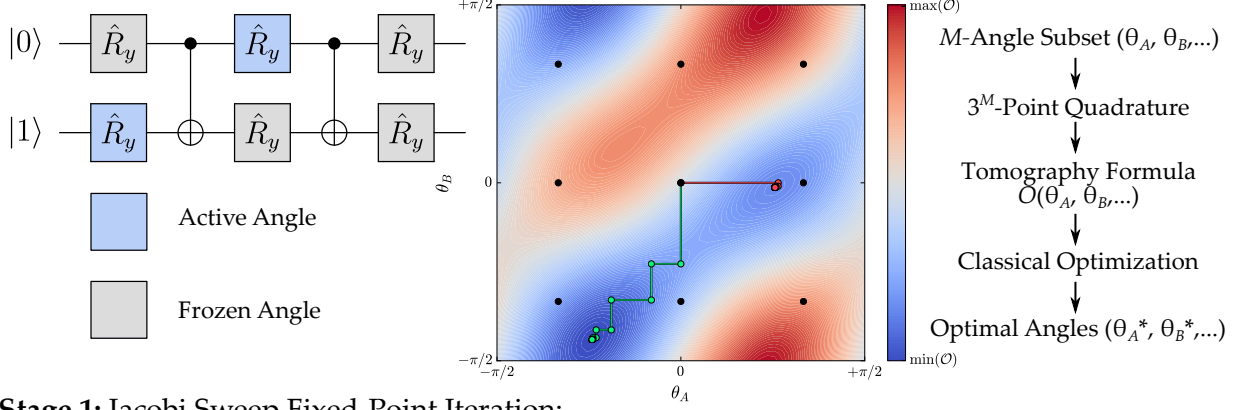
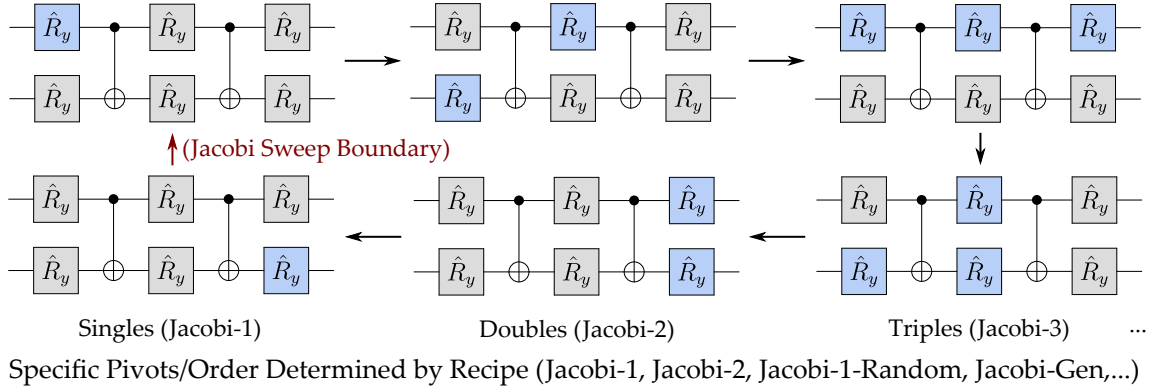


FIG. 1: Schematic of classical Jacobi diagonalization algorithm local move for pivot index (i, j) . A local 2×2 eigenproblem is solved at the (i, j) pivot index, determining a Givens rotation \hat{G} which explicitly zeros A'_{ij} . This alters the i -th and j -th rows and columns of the matrix \hat{A}' . Subsequently, the process is repeated in “sweeps” over different sets of (i, j) pivot indices. Each step reduces the off-diagonal weight of matrix \hat{A} , so the convergence is monotonic in an objective function defined as $O(\{\theta_{ij}\}) = +\sum_{i \neq j} A_{ij}^2$ or $O(\{\theta_{ij}\}) = -\sum_i A_{ii}^2$.

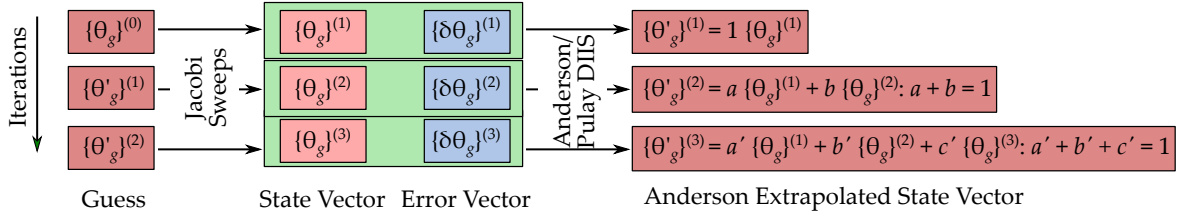
Local Jacobi Moves: Partial Tomography and Analytical Classical Optimization:



Stage 1: Jacobi Sweep Fixed-Point Iteration:



Stage 2: Anderson/Pulay DIIS Sequence Acceleration:



Anderson/Pulay DIIS Examine Iterative History to Account for Missing Couplings Between Parameters

FIG. 2: Overview of the family of Jacobi fixed point iteration plus Anderson/Pulay DIIS sequence acceleration algorithms developed for variational quantum circuit optimization in this work.

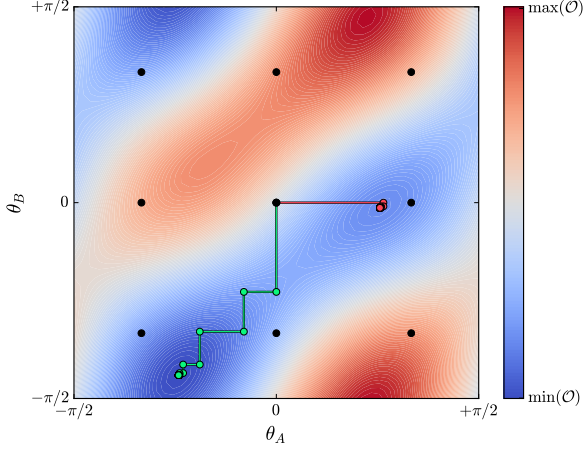


FIG. 3: Schematic of 9-point quadrature and classical Jacobi-1 optimization procedure for two-gate tomography. The observable expectation value $\mathcal{O}(\theta_A, \theta_B)$ is an example computed on a dense reference grid and depicted as the filled contour map. Sampling the observable on the 9-point quadrature grid depicted as filled black circles is sufficient to recover the analytical tomography formula of Equation 18. Subsequently, the optimal angles θ_A and θ_B can be found by classical optimization techniques, e.g., by the classical Jacobi-1 approach depicted in the green and pink lines. However, care must be taken to avoid spurious local minima which might be present, such as the solution found by the pink classical Jacobi-1 optimization.

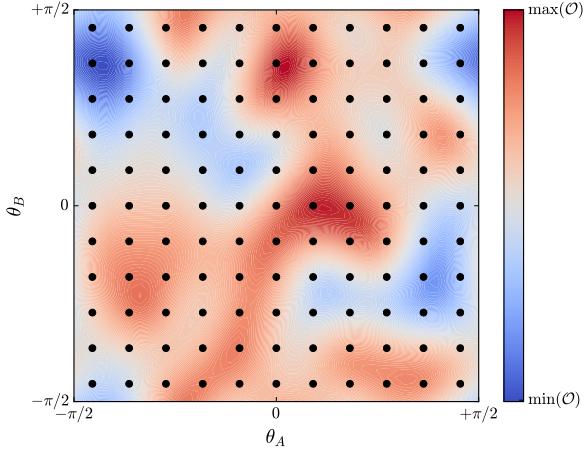


FIG. 4: Example of using Fourier quadrature for QAOA tomography ($M = 2$, $G_D = 5$). $(2 \cdot 5 + 1)^2 = 121$ quadrature points are required to analytically resolve the tomography coefficients.

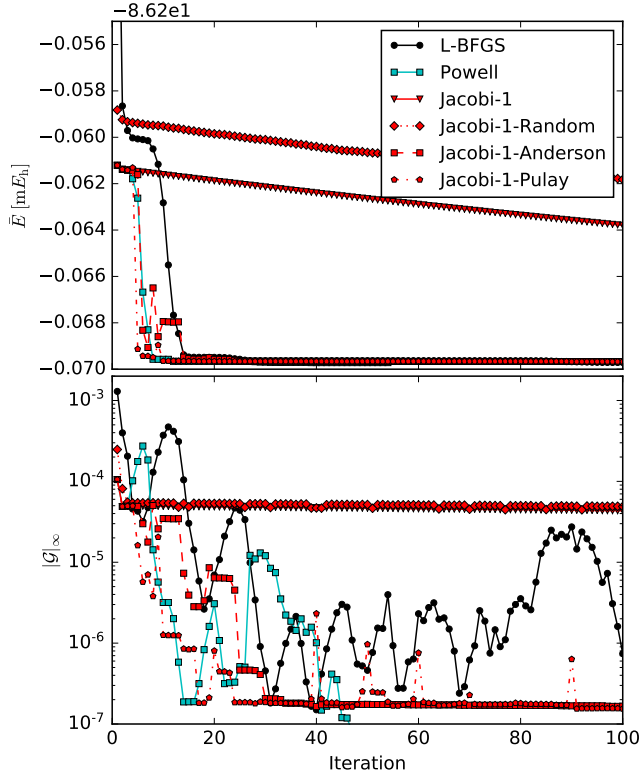


FIG. 5: State-averaged VQE energy convergence (top) and maximum gradient element (bottom) as a function of logical iteration count for the $N_{\text{state}} = 5$ “easy” test case. Jacobi-1 (all single angles) methods highlighted.

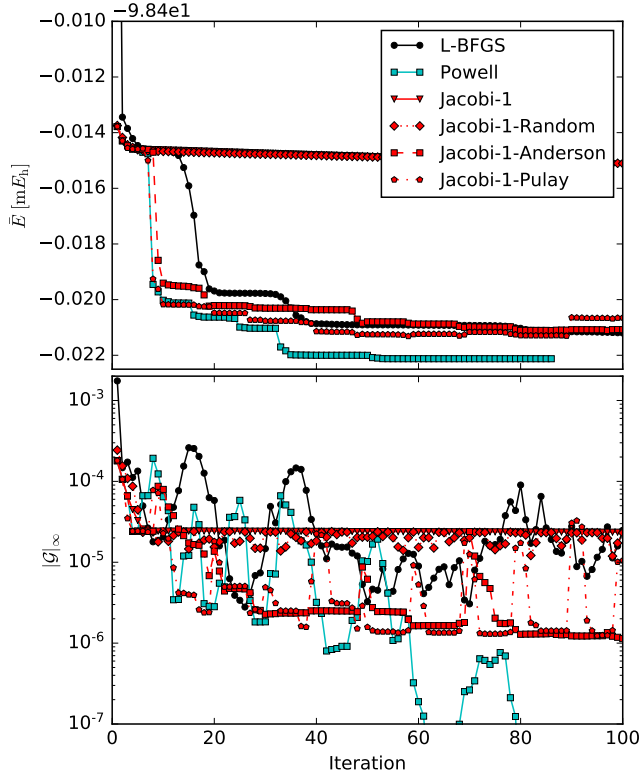


FIG. 6: State-averaged VQE energy convergence (top) and maximum gradient element (bottom) as a function of logical iteration count for the $N_{\text{state}} = 3$ “hard” test case. Jacobi-1 (all single angles) methods highlighted.

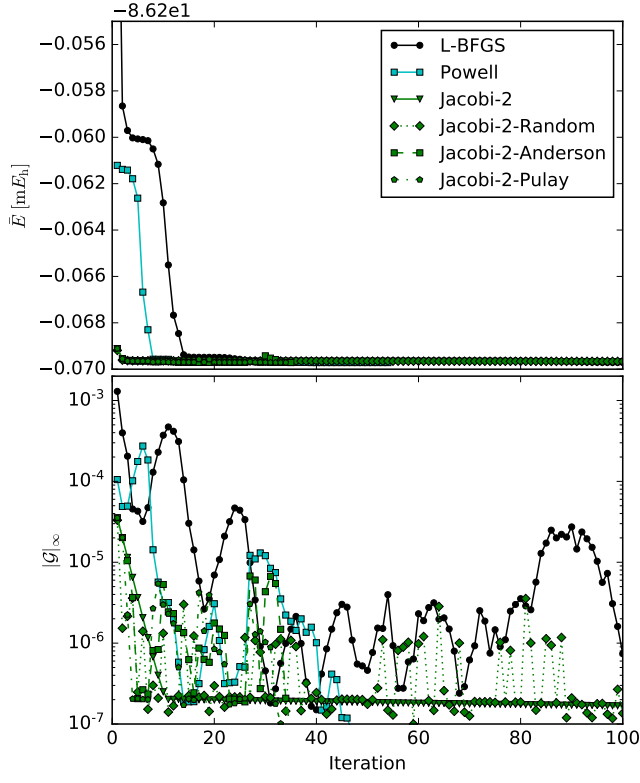


FIG. 7: State-averaged VQE energy convergence (top) and maximum gradient element (bottom) as a function of logical iteration count for the $N_{\text{state}} = 5$ “easy” test case. Jacobi-2 (all pairs of angles) methods highlighted.

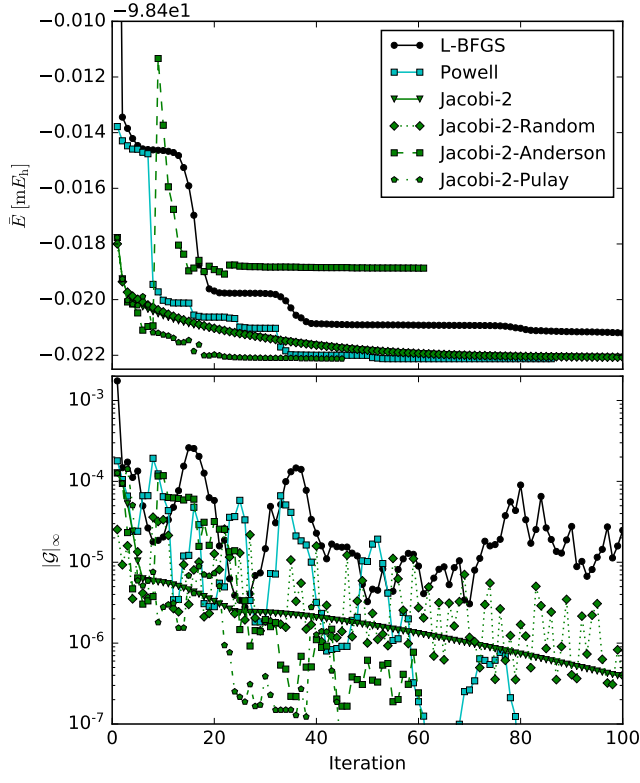


FIG. 8: State-averaged VQE energy convergence (top) and maximum gradient element (bottom) as a function of logical iteration count for the $N_{\text{state}} = 3$ “hard” test case. Jacobi-2 methods (all pairs of angles) highlighted.

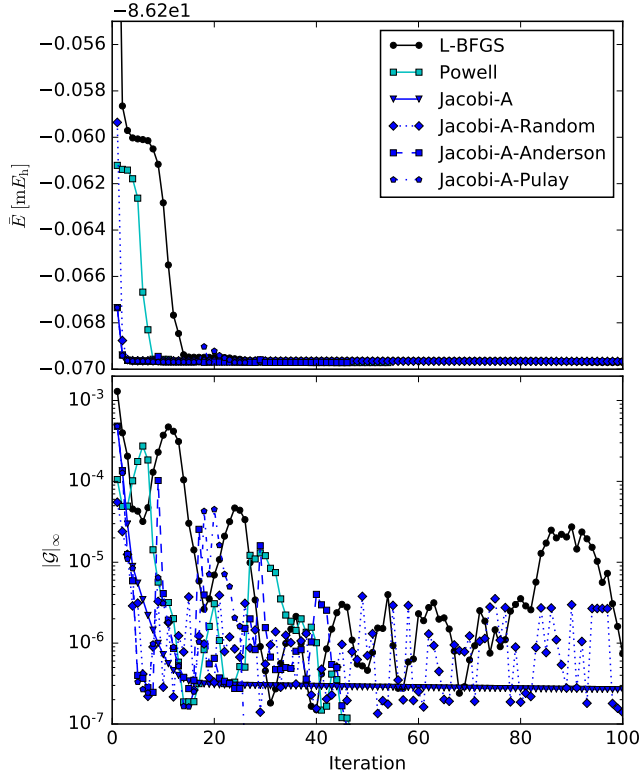


FIG. 9: State-averaged VQE energy convergence (top) and maximum gradient element (bottom) as a function of logical iteration count for the $N_{\text{state}} = 5$ “easy” test case. Jacobi-Gen “A” methods (all pairs of angles within single qubit wires) highlighted.

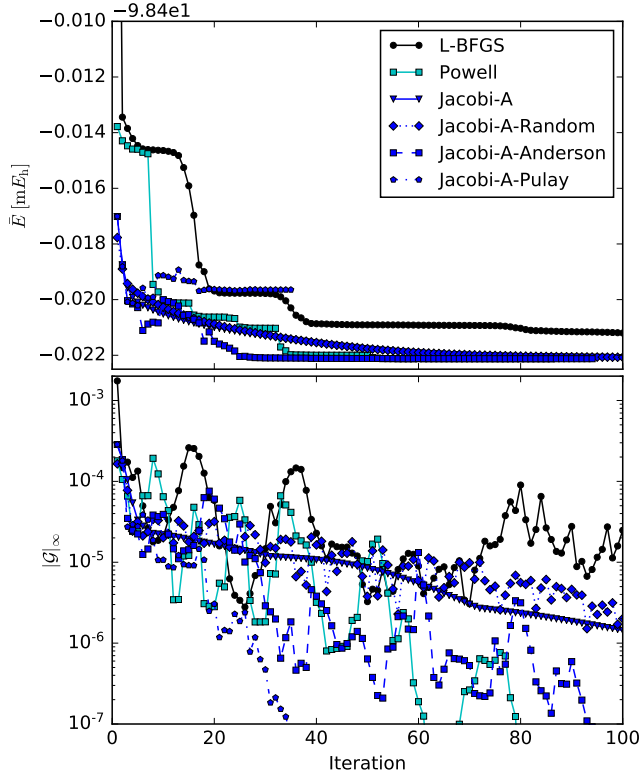


FIG. 10: State-averaged VQE energy convergence (top) and maximum gradient element (bottom) as a function of logical iteration count for the $N_{\text{state}} = 3$ “hard” test case. Jacobi-Gen “A” methods (all pairs of angles within single qubit wires) highlighted.

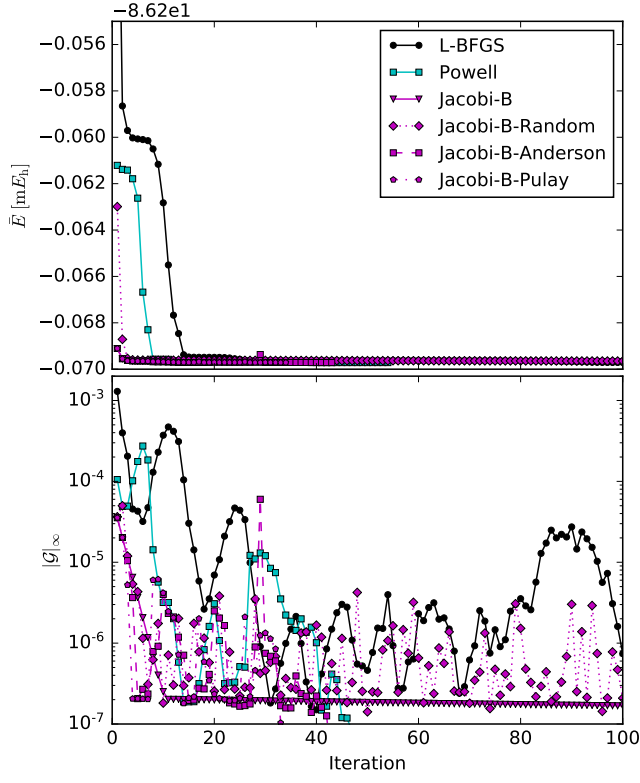


FIG. 11: State-averaged VQE energy convergence (top) and maximum gradient element (bottom) as a function of logical iteration count for the $N_{\text{state}} = 5$ “easy” test case. Jacobi-Gen “B” methods (all pairs of angles within single and on adjacent qubit wires) highlighted.

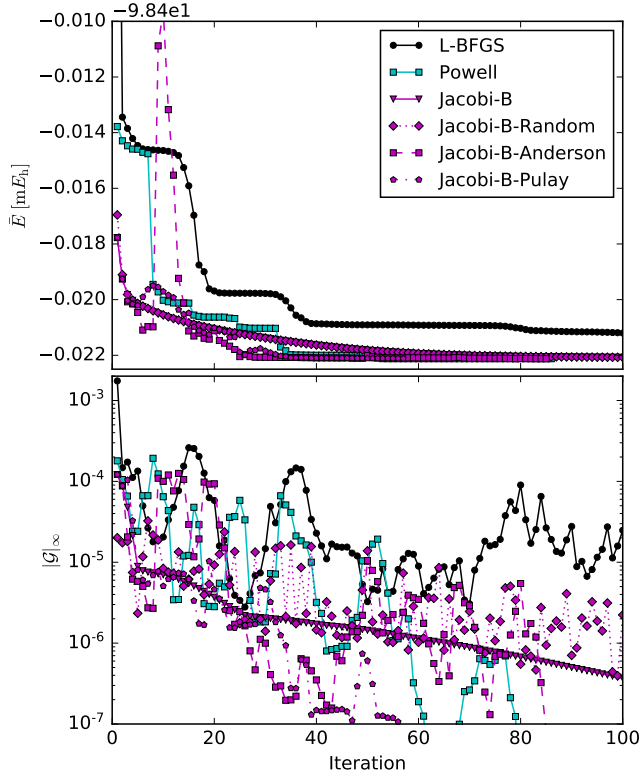


FIG. 12: State-averaged VQE energy convergence (top) and maximum gradient element (bottom) as a function of logical iteration count for the $N_{\text{state}} = 3$ “hard” test case. Jacobi-Gen “B” methods (all pairs of angles within single and on adjacent qubit wires) highlighted.

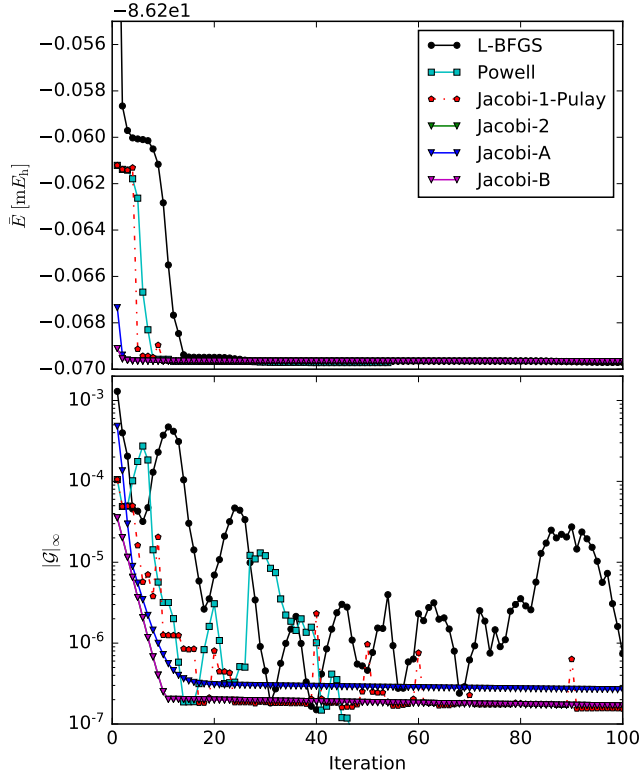


FIG. 13: State-averaged VQE energy convergence (top) and maximum gradient element (bottom) as a function of logical iteration count for the $N_{\text{state}} = 5$ “easy” test case. Jacobi-1-Pulay, Jacobi-2, Jacobi-A, and Jacobi-B methods compared to L-BFGS and Powell.

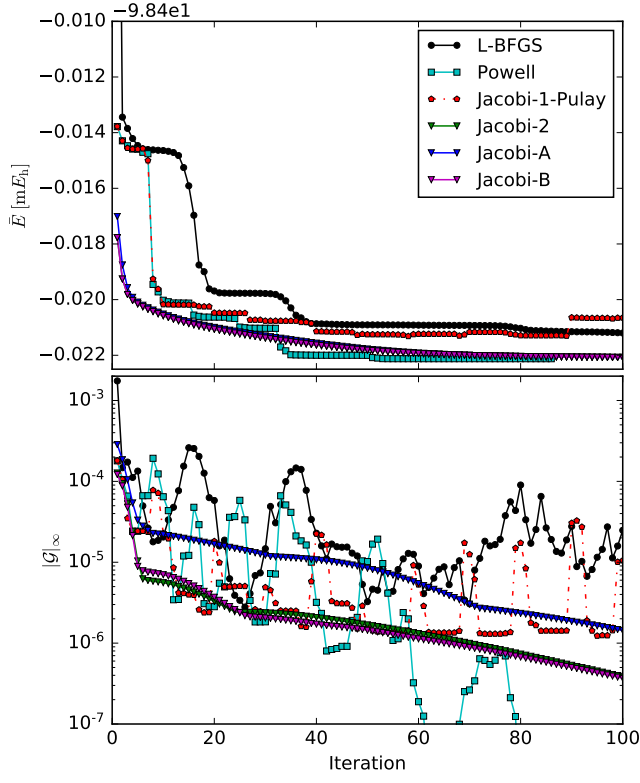


FIG. 14: State-averaged VQE energy convergence (top) and maximum gradient element (bottom) as a function of logical iteration count for the $N_{\text{state}} = 3$ “hard” test case. Jacobi-1-Pulay, Jacobi-2, Jacobi-A, and Jacobi-B methods compared to L-BFGS and Powell.

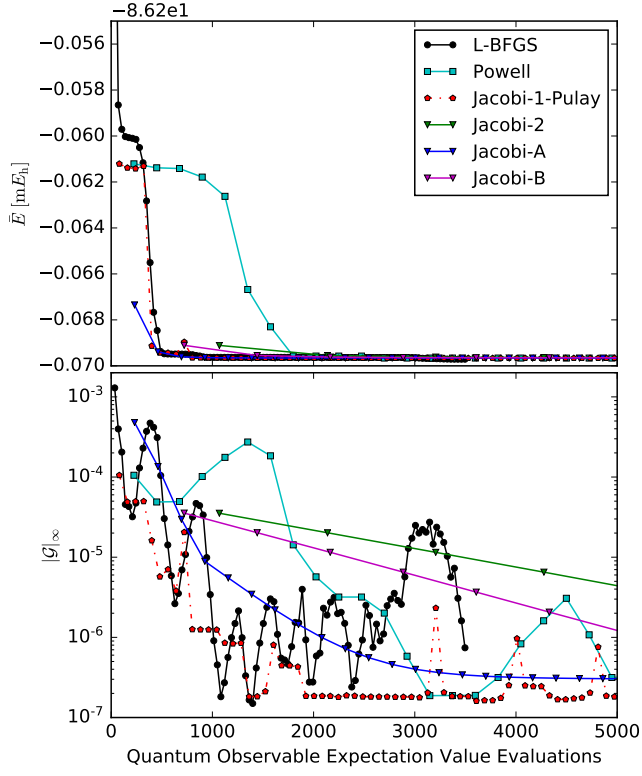


FIG. 15: State-averaged VQE energy convergence (top) and maximum gradient element (bottom) as a function of observable expectation value count for the $N_{\text{state}} = 5$ “easy” test case. Jacobi-1-Pulay, Jacobi-2, Jacobi-A, and Jacobi-B methods compared to L-BFGS and Powell.

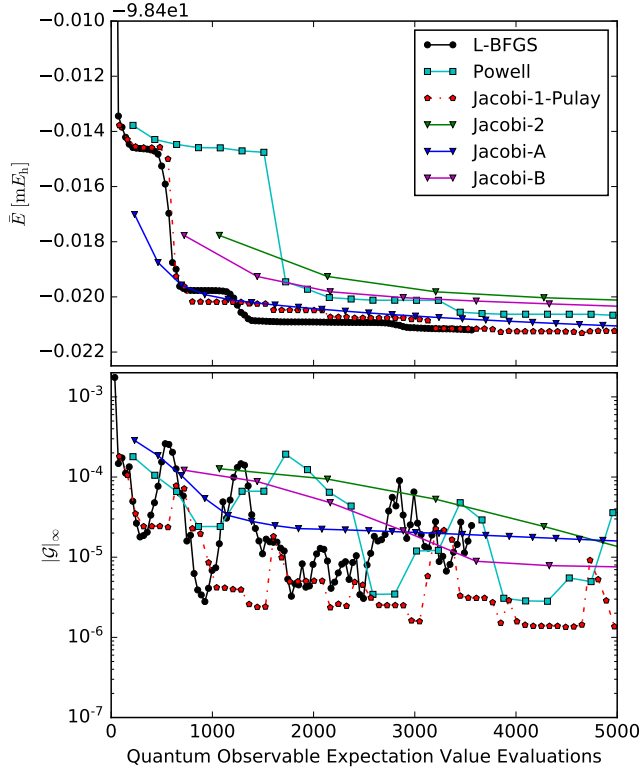


FIG. 16: State-averaged VQE energy convergence (top) and maximum gradient element (bottom) as a function of observable expectation value count for the $N_{\text{state}} = 3$ “hard” test case. Jacobi-1-Pulay, Jacobi-2, Jacobi-A, and Jacobi-B methods compared to L-BFGS and Powell.